Photoswitchable Binary Nanopore Conductance and

Selective Electronic Detection of Single

Biomolecules Under Wavelength and Voltage

Polarity Control

James T. Hagan¹, Alejandra Gonzalez², Yuran Shi^{2†}, Grace G.D. Han^{2*}, and Jason R. Dwyer^{1*}

1. Department of Chemistry, University of Rhode Island, 140 Flagg Rd., Kingston, RI, 02881.

Department of Chemistry, Brandeis University, 415 South Street, Waltham, Massachusetts
 United States

*gracehan@brandeis.edu, jason_dwyer@uri.edu

†current address: Department of Chemistry, Stanford University, 364 Lomita Drive, Stanford, CA 94305, United States

ABSTRACT. We fabricated photo-regulated thin-film nanopores by covalently linking azobenzene photoswitches to silicon nitride pores with ~10 nm diameters. The photo-responsive coatings could be repeatedly optically switched with deterministic ~6 nm changes to the effective

nanopore diameter and of ~3× to the nanopore ionic conductance. The sensitivity to anionic DNA and a neutral complex carbohydrate biopolymer (maltodextrin) could be photo-switched "on" and "off" with analyte selectivity set by applied voltage polarity. Photo-control of nanopore state and mass transport characteristics is important for their use as ionic circuit elements (*e.g.* resistors and binary bits) and as chemically tuned filters. It expands single-molecule sensing capabilities in personalized medicine, genomics, glycomics, and—augmented by voltage polarity selectivity—especially in multiplexed biopolymer information storage schemes. We demonstrate repeatably photo-controlled stable nanopore size, polarity, conductance, and sensing selectivity—by illumination wavelength and voltage polarity—with broad utility including single-molecule sensing of biologically and technologically important polymers.

Keywords

nanopore, silicon nitride, single-molecule detection, DNA, glycan, azobenzene, photoswitch

Solid-state abiotic nanopores capture the imagination and have emerged in applications as high-performance platforms for single-molecule science, as nanoscale apertures for fundamental physics experiments and controlled cargo delivery, as conductive and often rectifying ionic circuit elements, as high resolution model systems for nanoporous filters, and as robust, device-ready analogues and mimics of their proteinaceous brethren. ¹⁻⁶ In most of these undertakings a nanopore—a ~10 nm-diameter channel through a ~10 nm-thick membrane—is immersed in an ionic electrolyte and provides the only path for voltage-driven mass transport

between solutions on either side of the membrane. In the most prevalent application of single-molecule DNA sequencing, electrophoresis of a DNA strand through a nanopore alters the ionic current flow to give rise to characteristic signals that can be used to recover the DNA base sequence.⁷

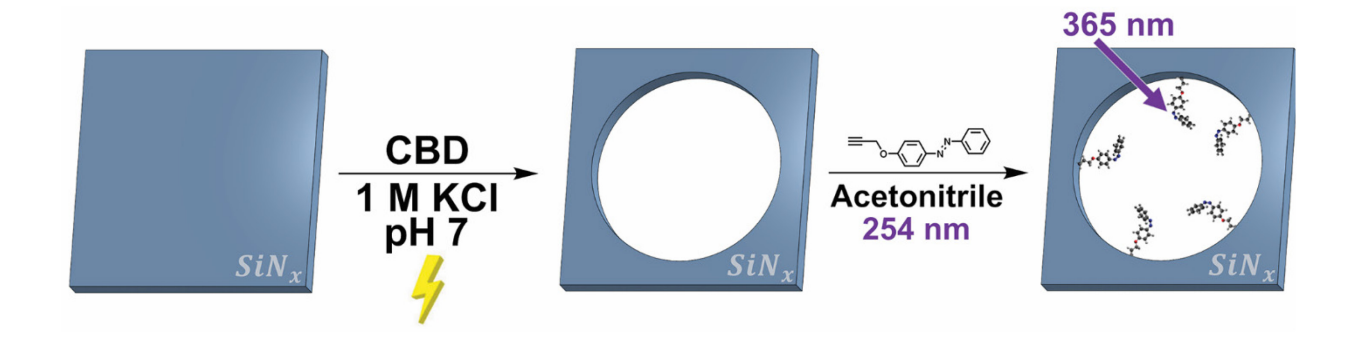
Photo-responsive nanopores are even more appealing than conventional pores. Nonlocal, noncontact, and wavelength-selectable control of photo-responsive nanopores can significantly enhance their properties and capabilities. Molecular photoswitches that respond to light by configurational isomerization are a prominent tool that can, when suitably coupled to a nanopore, be used to optically control aspects of its nanoscale structure and function. This approach is in contrast to those using conventional nanopores to give photoswitch-configuration-specific readout of target molecules or complexes functionalized with photochromophores.⁸⁻¹¹ Chemically derivatizing the nanopore surface, rather than the molecule, allows nanopore sensing to remain truly label-free, places the responsibility for chemical functionalization in the hands of the device fabricator rather than the practitioner, provides a fixed route to surface functionalization (vs. the myriad of approaches that might be required to derivatize different molecules), and decreases the time needed for sample preparation for nanopore sensing.⁵ At the same time, chemical functionalization of the nanopore rather than the molecule is better suited to applications, such as filtering or controlled delivery, that require the platform, itself, to deliver the desired structure and performance. Photoswitches including spiropyrans, ^{12, 13} hydrazones, ¹⁴ donor-acceptor Stenhouse adducts, ¹⁵ stilbenes, ¹⁶ and azobenzenes ^{17, 18} isomerize upon light irradiation, which leads to changes to their structure, polarity, and various electronic and photophysical properties. Such molecular-scale changes to the nanopore coating can have longerrange effects including altering interfacial properties (e.g. the Debye-layer) that in turn control

dynamic processes like nanoscale mass transport through the nanopore.^{3, 5, 19-22} They can thus modulate the sensing of the ion, small- and macromolecule, and nanoparticle and virus targets of nanopore sensing.

We chose both nanopore platform (silicon nitride) and photo-switch (azobenzene) to be robust and adaptable for a wide range of downstream applications. Low-pressure chemical vapor deposition (LPCVD) silicon-rich silicon nitride (SiN_x) is the most prevalent and conventionally versatile nanopore fabrication material supporting nanopores of a wide range of sizes. 1, 2, 5, 20, 23, 24 It is a standard material in microelectronics so that the integration of nanopores into complex devices can be conceived of alongside manufacturing at-scale. Azobenzenes, in particular, display facile reversible switching with alternating UV and visible light irradiation between the ground-state trans isomeric form and its metastable cis isomer counterpart (Figure S1). The cisto-trans (reverse) isomerization can be also promoted by thermal activation, offering an additional method of switching. Due to the ease of synthesis and derivatization, ²⁵ high cyclability of the photoswitching processes, ¹⁸ high isomerization rates, ¹⁷ and significant structural and polarity changes, ^{26, 27} the azobenzene derivatives are widely incorporated in various material systems, notably polymeric films, ²⁸⁻³⁰ nanoparticles, ³¹⁻³³ and cargo-containing vesicles. ³⁴ Configurational isomerization inside a zeptoliter volume such as a nanopore or in nanocages, nanoporous frameworks, or nano-cavities between aggregated nanoparticles³⁵—where even the solvent structure and energetics may be perturbed by confinement—is itself a rich area for investigation. We anticipated, however, that a suitable azobenzene covalently coupled to the surface of a thin-film nanopore (Scheme 1) and remaining photo-switchable would be able to effectively adjust the size and polarity of nanopore systems. We first assessed whether we could reliably photoselect each azobenene configurational isomer and what the resultant nanopore

properties would be. We then challenged azobenzene-festooned nanopores with two analytes—DNA and the complex carbohydrate maltodextrin. Each presented distinct physicochemical properties to the nanopore and each was drawn from a molecular class core to pursuits within genomics and glycomics, respectively.^{5, 19, 36}

Scheme 1. Formation and coating of SiN_x nanopores. Nanopores were fabricated by voltage-induced controlled (dielectric) breakdown (CBD) in buffered electrolyte and then covalently functionalized with the azobenzene photoswitch by photohydrosilylation in acetonitrile using 254 nm light. Longer wavelengths of light present in unfiltered mercury lamps can drive $trans \rightarrow cis$ isomerization.



RESULTS AND DISCUSSION

The 4-(propargyloxy)azobenzene reversibly photo-switched for more than 100 cycles in free solution (Figure S2). The half-life of the metastable *cis* 4-(propargyloxy)azobenzene in free solution at room temperature was 61 h in the organic solvent (acetonitrile) used for photo-switching and 41 h in the aqueous electrolyte (1 M KCl/10 mM HEPES) used for characterization measurements (Figure S3). We therefore expected no (bulk) solvent-induced

impediments to photochemically and thermally stable isomerization of our nanopore coating. The nanopore itself, however, may present barriers to photo-switching from confinement, surface curvature, or interactions with the inorganic surface. Unlike a photochromic coating on the outer surface of a nanoparticle,^{37, 38} for example, where the free end of the molecule is further away from its neighbors, the attachment of a molecule inside a nanopore means that the free ends of the molecule will all tend to be more sterically crowded than at the surface. Interactions arising from crowding in dense films may also affect the nature of the photoswitching.

A SiN_x nanopore of (original) diameter d_{SiN_x} coated with a molecular film of thickness $t_{\text{film}}^{cis/trans}$ will have a physical diameter of $d_{\text{film}}^{cis/trans} = d_{\text{SiN}_x} - 2 \cdot t_{\text{film}}^{cis/trans}$ with t_{film}^{trans} up to 1.47 nm and t_{film}^{cis} up to 1.05 nm (Figure S1, 1). Nanopore dimensions dominate the nanopore conductance, G, in molar ionic strength solutions

$$G = \sigma \left(\frac{4l}{\pi d^2} + \frac{1}{d}\right)^{-1} \tag{1}$$

where d and l are the nanopore diameter and length, respectively, and σ is the solution conductivity. The nanopore conductance is then dependent on the cis- vs. trans-dependent thickness of the surface coating. All current (and thus conductance) measurements were performed in the dark. The measured conductances before and after the installation of a film or after a photochromic reaction can then be used to infer the film thickness ($t_{\rm film}^{cis/trans} = \frac{1}{2}(d_{\rm SiN_x} - d_{\rm film}^{cis/trans})$) or change in film thickness ($|\Delta d_{\rm film}| = 2|t_{\rm film}^{cis} - t_{\rm film}^{trans}|$), respectively. The functionalized nanopores showed reversible photo-switching between a high and a low conductance state (Figure 1, Figure S4) as would be expected from cycling of the film thickness between $t_{\rm film}^{trans}$ and $t_{\rm film}^{cis}$ (Figure 1) and the conductance between G_{trans} and G_{cis} . The high

conductance state was induced by 365 nm light—the wavelength that drives the *trans* $\rightarrow cis$ isomerization that would increase the pore diameter and conductance (by Equation 1). The low conductance state was induced by visible light—this excitation drives the *cis*→*trans* isomerization reaction that would decrease the pore diameter and conductance. The conductance data and wavelength-dependence of switching show that the pore coating is initially predominantly in the cis configuration despite using the more energetically stable trans isomer for photohydrosilylation. Separate bulk solution-based experiments show that the spectrum of the unfiltered mercury lamp used for photohydrosilylation could also drive *trans→cis* isomerization (Figure S5), albeit at a low $\sim 20\%$ trans $\rightarrow cis$ conversion yield in bulk solution (~ 55 mM). The apparent enrichment of the cis content of the surface coating over the bulk could be explained by the more hydrophilic nature of the cis isomer (vide infra) causing preferential transport to, or partitioning into, the nanopore interior when compared to the trans isomer. It could also be explained by the more prosaic mechanism that an initial trans film is converted to the cis form over the course of the photoirradiation. With the surface coating in place the reversible cycling of photo-induced changes in conductance is in accord with the photochemical reaction mechanism in Figure 1 and convincingly supports the successful formation of a photochromic SiN_x nanopore.

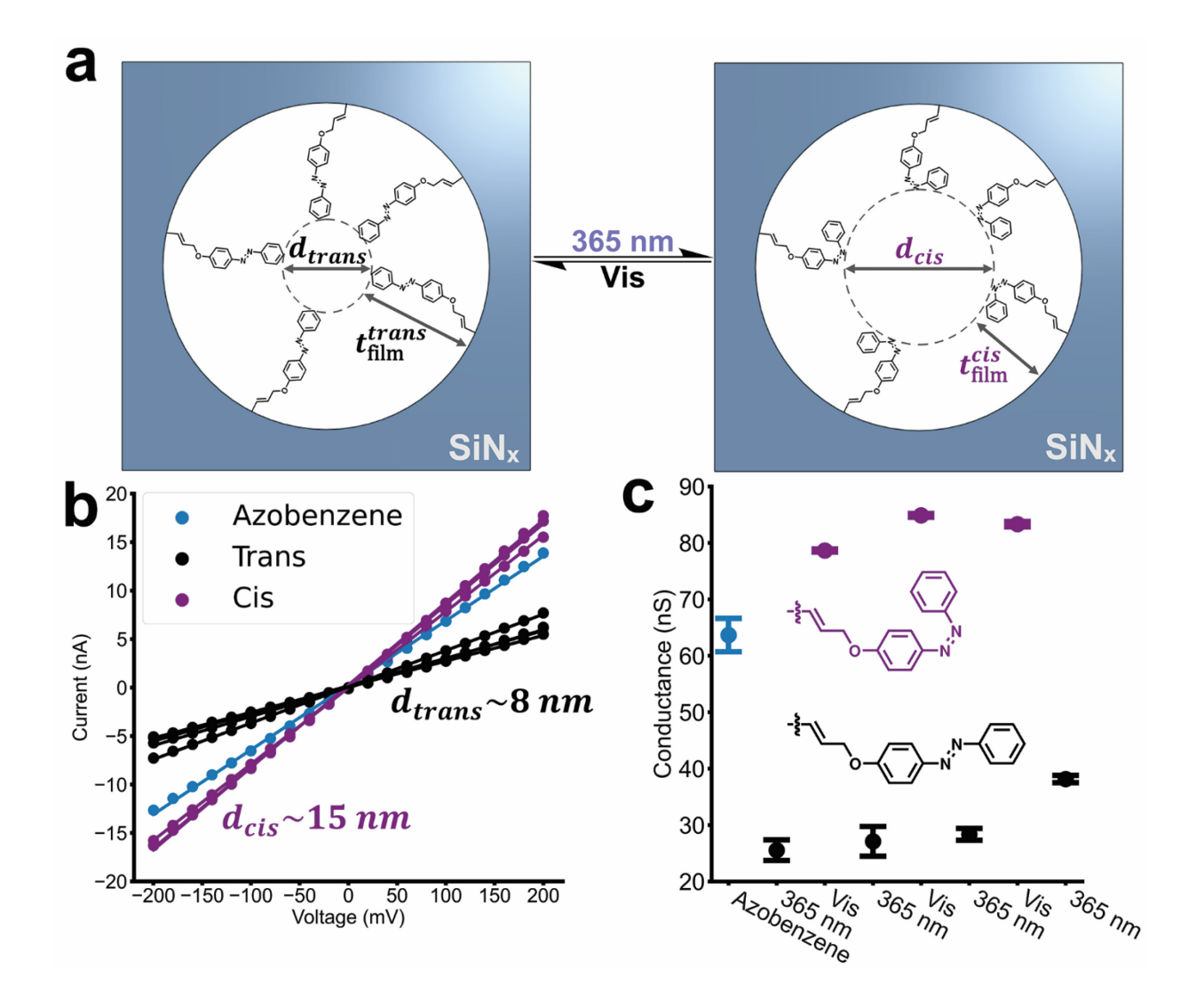


Figure 1. (a) Photoswitching of the azobenzene film coating by 365 nm (UV flashlight, $trans \rightarrow cis$) and white light source ($cis \rightarrow trans$) should drive physical changes in monolayer effective thickness and thus nanopore diameter (dashed circle). Photoirradiation was ceased prior to measuring currents. (b,c) The initial conductance of the nanopore after coating ("azobenzene") was recorded before the photoswitching experiments with the conductance measured after each photoirradiation step. The measurements revealed two statistically significant conductance states.

The average conductance-derived diameter change (Equation 1) upon installation of the 4-(propargyloxy)azobenzene was $\bar{d} \pm \sigma = 1.8 \pm 1.3\,$ nm (8 independent pores), corresponding to a ~1 nm film thickness. This is consistent, within typical measurement accuracy 20, 40, 41 with the installation of no more than a monolayer of primarily cis-4-(propargyloxy)azobenzene (t_{film}^{cis} = 1.05 nm, Figures 1, S1). Wetting effects, surface coverage variability (vide infra), and differences in relative cis/trans enrichment could account for the range of initial apparent film thicknesses. Comparison of Figures S4 and S6 shows that despite this initial variability all of the functional coatings could be definitively and controllably photo-switched between two readily distinguishable high and low states. Switching between the 1.47 nm trans film thickness and the 1.05 nm cis film thickness (Figures 1, S1) would change the physical nanopore diameter by 0.84 nm and this would change the conductance in accordance with Equation (1). The mean conductance-derived diameter change, derived with Equation (1) and the conductance changes across 8 independent pores was $\Delta d_{\text{switch}} = 6.3 \pm 1.1$ nm. This corresponds to a ~3 nm change in apparent film thickness accompanying the cis/trans isomerization, approximately 7× the magnitude expected from the change in molecular dimensions. In earlier nanopore surface coating work, ²⁰ 4× greater increases than the molecular dimension in conductance-derived film thickness were ascribed to increases in the hydrophobicity of the surface coating. We present density functional theory (DFT) calculations below that show that the trans isomer is indeed more hydrophobic than the cis isomer, so that the numerical discrepancy does not compromise the validity of the connection of conductance switching to molecular isomerization but rather underscores the importance of wetting in the often challenging nature of nanoconfined chemistry. 42, 43 When nanopore coatings are hydrophobic, the diameter calculated from the conductance using Equation (1) is better treated as an effective diameter—incorporating size and wetting—than a physical diameter. Importantly, this complication highlights that this solid-state photochromic nanopore may be useful as a platform not just for applications but for exploration of such fundamental phenomena.

The 4-(propargyloxy)azobenzene moiety offers two distinct nanopore coatings without change of chemical formula or molecular structure other than isomerization about a double bond. Unlike for some photochromic species such as spiropyrans, there is no change in the discrete formal charges on the molecule during isomerization in the pH range of interest (pKaH transazobenzene -2.95,44 cis-azobenzene -1.4945). Each configuration of the azobenzene, however, presents a different charge distribution (Figure S7) at the interface between the nanopore surface and solution—and to any proximal analyte molecule. The consequences of isomerization thus transcend geometry. The trans isomer is largely hydrophobic with a dipole moment of 2.1 D whereas the cis isomer is more hydrophilic with a dipole moment of 3.9 D, according to DFT calculations of each isomeric structure. This large polarity change of the azobenzene coating will affect the nanopore wetting, in accordance with previous reports where the photo-isomerization of surface-functionalized azobenzene changed the contact angle of liquid on the surface. 46-48 In addition, 4-(Propargyloxy)azobenzene in the lower energy state (trans) has limited solubility in aqueous solutions, as confirmed by the strongly reduced solution absorbance in the UV-vis spectra (Figure S8a). The solid undergoes UV-induced isomerization and then, as a result of the increased hydrophilicity of the cis isomers, undergoes subsequent dissolution in the aqueous solution. The absorption spectrum of the cis species in aqueous solution displays the characteristic absorption bands of a cis state (π – π * at 310 nm and n– π * at 430 nm) consistent with those recorded in organic solutions (Figure S8b). The solubilized cis isomers switch back to trans upon white light irradiation and immediately precipitate (Figure S8a). Thermal activation

at 75 °C also leads to the facile reversion to *trans* which precipitates upon cooling to room temperature (Figure S8c). These observations in bulk solution are useful to provide insight into how the properties of each isomer could affect the interface between the surface coating and the confined ionic solution. Differences in nanopore wetting can affect the apparent nanopore size in ways not explicitly accounted for in Equation (1) where the more hydrophobic *trans*-azobenzene-coated nanopore appeared smaller than would be explained by the molecular dimensions, alone (*vide supra*). The effect of coating-induced restructuring of the nanopore-entrained electrolyte could be accounted for by an effective solution conductivity in Equation (1). The hydrophilicity difference between the two isomers also offers a physicochemical basis for the apparent *cis* enrichment of the nanopore coating upon photohydrosilylation (*vide supra*). In spite of the potential and observed solvation complexities we could reversibly switch the photochromic pore in pure water (Figure S9) and without (conductance-inferred) differences in photoisomerization reaction endpoints *versus* acetonitrile.

An unfunctionalized SiN_x nanopore surface is comprised of a mixture of surface —OH and —NH₂ groups that make it neutral at pH ~4.3 (by —O⁻ and —NH₃⁺), positively charged at more acidic pH (by —OH and —NH₃⁺) and negatively charged at larger pH values (by —O⁻ and —NH₂).^{20, 49} This change in surface charge with pH changes the conductance at the same time.²⁰ For SiN_x, there would be a minimum in the conductance at the isoelectric point (pI ~4.3) with the higher conductance values at more and less acidic pH values when the surface is charged. We measured the conductance of the same photochromic nanopore in both configurations as a function of pH (Figure S10a,b). The transition between two regions of opposite slope, coupled with measurements using maltodextrin at pH 7 (*vide infra*)¹⁹, indicate a positively charged surface in the less acidic region for the *cis* pore. The measured curves show no dramatic

departure from the general behavior of the bare SiN_x pore surface. In addition, *cis* 4(propargyloxy)azobenzene was observed to be stable at pH 3 over 110 minutes (Figure S10c) supporting the robustness of the *cis* pores and studies performed at low pH conditions. Since the 4-(propargyloxy)azobenzene is neither acidic nor basic and does not form charged species within pH 3-7, ⁵⁰ it is more likely that the surface coating density is insufficient to prevent the underlying chargeable SiN_x from being exposed to solution and then contributing to the pH-dependent conductance. This is in contrast to earlier work with short (compact) alkyl chains where it was the surface coating properties that dictated the change of conductance with pH, with no indication of exposed SiN_x. ²⁰ The *trans* film will create a more hydrophobic local surface environment for any unprotected SiN_x and the smaller pore diameter will amplify its influence on the nanoconfined solution structure which is the means by which the surface charge is detected through conductance. This local hydrophobic environment could explain why the experimental *cis* and *trans* curves are shifted relative to each other and the curve for the *trans* film showed less concordance with the curve for bare SiN_x than the *cis* film.

We created nanopores with photoselectable size, polarity, and conductance and, importantly for applications, reliable and stable operation. Photo-cycling between the two distinct low (*trans*) and high (*cis*) conductance states of the pore was done in discrete experimental steps—photo-switching in acetonitrile buttressed by conductance measurements in aqueous electrolyte before and after—that demonstrated both the reversibility and the robustness of the photochromic nanopores to solvent exchange and mechanical handling. Redox-mediated electrocatalytic Z-to-E reversion processes require higher voltage conditions, at least 1 V *versus* Fc/Fc⁺, than the 200 mV used in this work.⁵¹ Significantly, the two distinct conductance states, supporting up to ~20 nA current flows through the pore, were stable across the 30 min

measurement time and in the presence of high electric fields (up to ~200 mV/15 nm\(\text{2}\)13 mV/nm) across the nanopore. Isomerization switching persisted over 2 weeks before declining in reliability. It is thus clear that we had successfully created a photochromic thin-film nanopore that maintained the metastable states, trans and cis, during and across several measurement periods. Such a nanopore can be used as a digital bit for reversible nondestructive data storage with readout of the state by ionic conductance and setting of the state by photons of the appropriate wavelength.⁵² A photochromic nanopore may also offer technical advantages as the photo-switchable readout element for DNA (and other biopolymer) data storage schemes. 1, 53, 54 For example it may offer the ability to turn readout off until switched on, or to read the same biopolymer through two different states of the same pore for added signal discrimination. We are also interested in the potential biomedical applications of the photochromic nanopore, in particular for biopolymer characterization and sequencing in the domains of genomics and glycomics.^{5, 7, 24, 36} The complex carbohydrates can take on a greater range of chemical composition, charge, and structure than DNA and this overall biopolymer diversity can be exploited at this exploratory stage to help characterize the photochromic nanopore, itself.¹⁹

For biopolymer analysis by conventional resistive-pulse nanopore sensing the nanopore must deliver fixed size and stable baseline current in the absence of analyte, and the analyte must be able to perturb the open-pore current. Both *cis* and *trans* pores gave steady baseline currents suitable for single-molecule sensing and consistent with a structurally stable surface coating (Figures 2, S11, and S12). Noise characteristics were similar to those from unfunctionalized silicon nitride nanopores (Figure S13). Single-molecule-characteristic discrete blockages could be detected for both DNA (+200 mV) and maltodextrin (-200 mV) with the pore in the *cis* configuration (Figures 2, S12) but the *trans* pore was nonresponsive to both, regardless of

applied voltage polarity ($\pm 200 \text{ mV}$; Figures 2, S11). The distinct current blockage transients for the *cis* pore—downward spikes for DNA and upward spikes for maltodextrin in Figure 2—were isolated by thresholding against the temporally local average current and representative examples are shown in Figures 2 and S14.⁵⁵ A more comprehensive representation of the 418 events (DNA) and 761 events (maltodextrin) is given in Figure 3. The average shifted histogram (ASH) plot of the change in nanopore conductance (ΔG) induced by passage of DNA through the pore, for example, shows multiple peaks that are consistent with passage of non-linearized DNA. The overall signatures of these events are typical of nanopore sensing of DNA and maltodextrin using unfunctionalized silicon nitride nanopores (Figure S15, S16) so that we can conclude that these photochromic nanopores are useful for profiling these two biopolymers with the additional capability of photo-controllable responsivity.^{19,56}

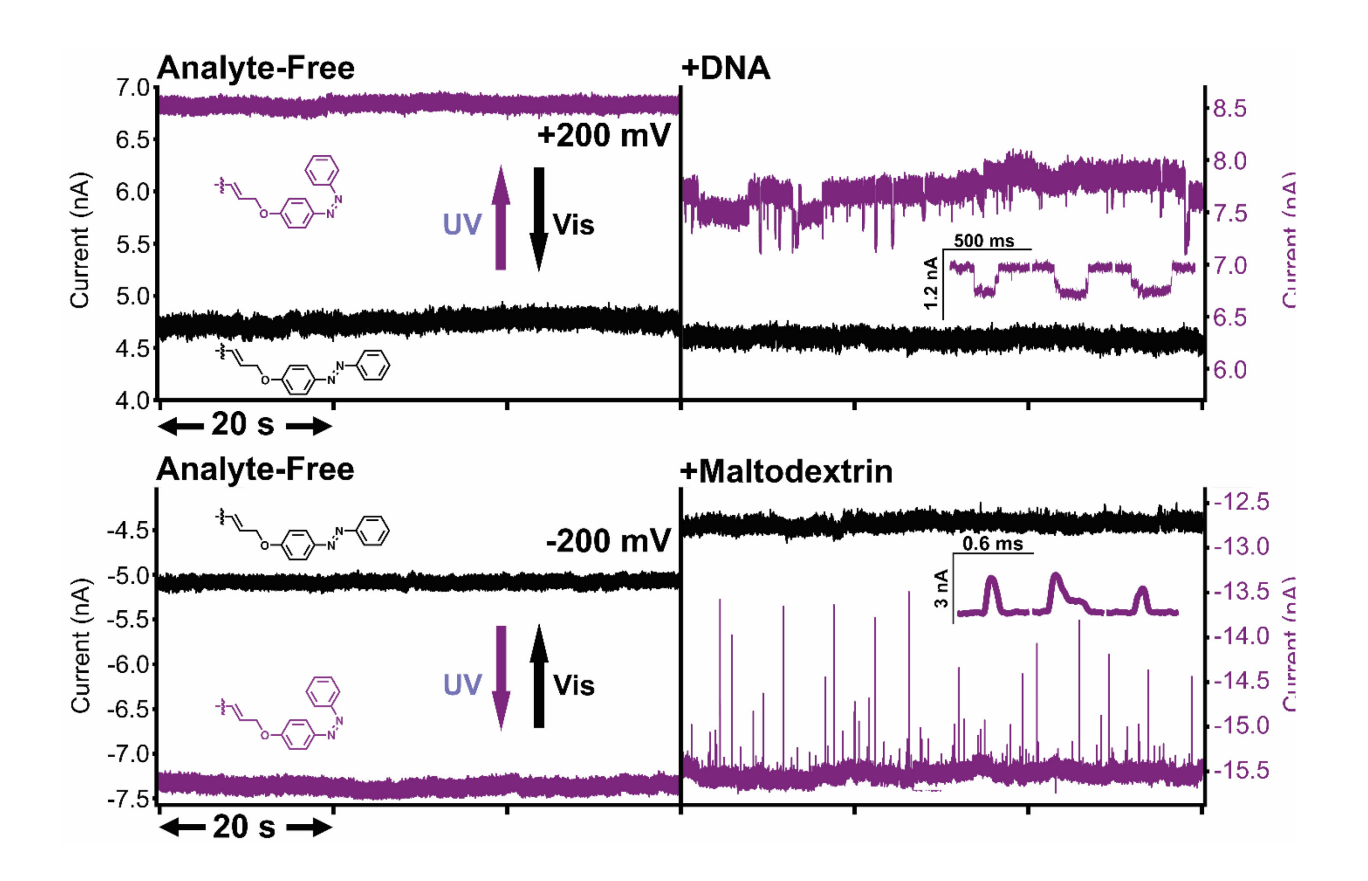


Figure 2. The *cis* and *trans* configuration of the nanopore coating turned the nanopore sensing on and off for two different molecules: maltodextrin, a neutral complex carbohydrate polymer, and 3 kbp dsDNA, an anionic biopolymer. The nanopores were isolated from the corresponding light sources after photoswitching. Current traces were acquired at +200 mV for DNA with a 10.1 nm (7.2 nm) diameter *cis* (*trans*) configuration pore and at -200 mV for maltodextrin with a 14.9 nm (7.6 nm) diameter *cis* (*trans*) configuration pore. Absence of analyte gave a steady baseline current. Addition of analyte to the pores with monolayer in the *cis* configuration resulted in readily detectable current spikes characteristic of that analyte. No such single molecule detection events were apparent with the coating in the *trans* configuration. Several representative events are shown as an inset.

The voltage polarity to detect DNA in these experiments is consistent with net transport in the direction of electrophoretic motion, as is generally the case for nanopore DNA sensing. ⁵⁶ A reduced and unsteady baseline current is common in DNA sensing using unfunctionalized SiN_x nanopores. ^{19,57} It is generally ascribed to "sticking" of the DNA to the nanopore surface and a plethora of surface chemical approaches have been developed to prevent such sticking. ^{19,21,41} While the 4-(propargyloxy)azobenzene coating does not prevent occasional sticking, further modification of azobenzene moiety with various functional groups, *e.g.* fluorous groups, could chemically tune this behavior without sacrificing the photo-switchability. ⁵⁸⁻⁶⁰ In an electrokinetic sense, maltodextrin is the antithesis of DNA: it is neutral and therefore nonresponsive to electrophoresis. Instead, transport—and thus sensing—of maltodextrin occurs *via* electroosmosis that requires a charged nanopore surface. ^{5,19,56} The voltage polarity for sensing maltodextrin—opposite to that of electrophoresis for anionic DNA—indicates a negative surface charge. An incompletely covered SiN_x surface, such as that suggested by the data in

Figure S10, would be terminated with —O and —NH₂ and thus be negative at the sensing pH of 7.^{20, 49} The consequence of nanopore photo-switching and analyte-specific electrokinetic transport mechanism means that to successfully detect the biopolymer of interest required photoswitching the nanopore to the correct *cis* configuration and setting the voltage to the analyte-specific voltage polarity.

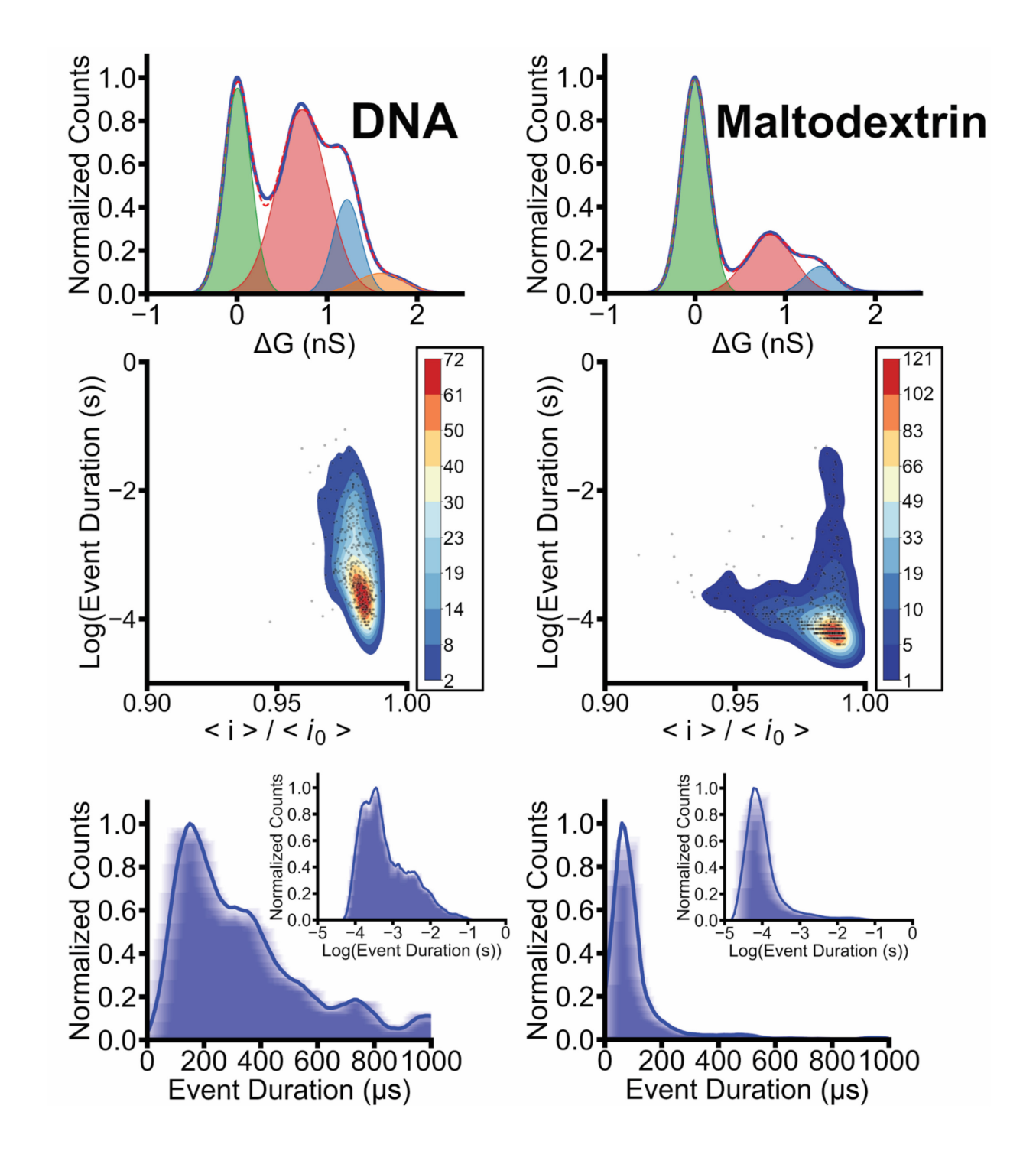


Figure 3. We sensed 3 kbp dsDNA using a 10.₁ nm diameter *cis* nanopore at 200 mV and maltodextrin using a 14.9 nm *cis* nanopore at -200 mV. All measurements were in 1 M KCl buffered to pH 7 with 10 mM HEPES. Top row. The average shifted histogram (ASH) of the

change in the conductance shows peaks corresponding to the open-pore current at $\Delta G = 0$ nS and analyte-induced blockages (peaked at $\Delta G > 0$). Discrete events were first extracted by thresholding from the baseline and ΔG is measured for each event relative to its local baseline. The shaded curves are fits to the experimental data. Middle row. Scatter plots of all isolated events are superimposed with heat maps showing the frequency of events in each analyte. The abscissa, $\langle i \rangle / \langle i_0 \rangle$, is the mean blockage of each event scaled by the mean open pore current proximal to the event. Bottom row. ASH plots of event duration for all isolated events peak at ~150 and 60 µs for DNA and maltodextrin, respectively.

The photochromic nanopore is nonresponsive to DNA at the voltage polarity where it is responsive to maltodextrin (-200 mV) because the electroosmotic driving force is insufficient to overcome the opposing electrophoretic driving force. Electroosmotic flow can be moderated by electrolyte salt composition and by surface chemical tuning 19-21, 49, 56—by pH as suggested by Figure S10 or by surface coating derivatization introduced above in the context of creating non-stick surfaces. There are thus additional, chemical parameters for tuning nanopore responsivity and selectivity in addition to the wavelength and voltage polarity. The broad similarity of conductance vs. pH curves for *cis* and *trans* configurations suggests that it is not a loss of nanopore surface charge at pH 7 that makes the *trans* nanopore nonresponsive to the neutral maltodextrin. Rather, the loss of response to both analytes suggests an origin in the physical size of the pore and hydrophobicity differences. Owing to the hydrophobic nature of the *trans* coating, the *trans* nanopores are physically smaller than in their corresponding *cis* configuration, but not physically as small as the 7 nm conductance-derived diameter would suggest (*vide*

supra).²⁰ We fabricated unfunctionalized, readily wetting, CBD SiN_x nanopores where Equation (1) can be used to calculate a physical nanopore diameter—here, at 5 nm smaller than even the effective diameter of the *trans* nanopore. We could readily detect both maltodextrin and DNA in these small nanopores (Figures S15 and S16), thus elevating the influence of the trans nanopore hydrophobicity on the sensing selectivity. To investigate this, we added an organic solvent, acetonitrile, to our electrolyte and attempted to sense both molecules in this new medium. We chose acetonitrile because the free trans 4-(propargyloxy)azobenzene (with alkene terminus) was soluble in acetonitrile at room temperature when it was insoluble in electrolyte (Figure S8). We were able to detect discrete events in the presence of both analytes at the analyte-specific voltage polarities corresponding to detection in Figure 2, thereby giving strong indications of the importance of nanopore coating hydrophobicity in an aqueous medium in determining the sensing selectivity. Electrolyte composition thus emerges as an additional potential parameter for tuning nanopore selectivity. Photoswitchable translocation in the photochromic nanopores can be useful as a molecular delivery system. For biopolymer data storage schemes, photo-switching can turn the detector on or off and voltage determines which biopolymers will be read out. Multiplexed data storage using two different biopolymers can increase the information storage density and the same photochromic pore can be used for readout with voltage polarity used to select the polymer of choice.

CONCLUSIONS

We have successfully created a metastable, stimulus-responsive nanopore using a conventional thin-film material used at scale in consumer microelectronic devices. The robust photoswitch continued to function even under confinement inside the pore, after measurements, and across weeks. The pore could be reversibly switched over repeated cycles between a smaller,

lower-conductance state and a larger, higher-conductance state accompanied by other changes such as to the surface coating polarity. These pores are practicable for applications even at the level of geometric aperture (e.g. high throughput chemically-tuned filtering) and ionic circuit element (e.g. as photoswitched conductor and digital bit). The more striking application vistas emerge from the ability to use light to switch between on/off single-molecule responsive states of the nanopore, and the ability to use voltage polarity to switch between biopolymer class (foreshadowing multiplexed molecular data storage possibilities). The proof-of-principle results for photoswitchable DNA sensing point to opportunities in exploring how to tailor the photochromic coating—by derivatization or class—to optimize both nanopore sensing performance against clogging, for example, and switching capability. Single-molecule sensing results for the glycan maltodextrin were comparable to those using a conventional SiN_x nanopore when photoswitched from the nonresponsive state, speaking to the general utility of this photochromic solid-state pore. We have, in sum, developed a thin-film platform—with diverse control parameters—for studying, tuning, and harnessing photoresponsive mass transport in diverse domains from filtration to single-molecule sensing of importance to the grand visions of information storage, genomics, and glycomics.

METHODS

Nanopores were formed by controlled (dielectric) breakdown (CBD)^{23, 61} in 15 nm-thick SiN_x membranes and then functionalized with custom synthesized 4-(propargyloxy)azobenzene by photohydrosilylation in acetonitrile (Scheme 1)²⁰. All characterizations of and measurements using the photochromic nanopores were performed using a Teflon housing inside a Faraday cage that blocked ambient light and in conventional 1 M KCl aqueous electrolyte buffered to pH 7 with 10 mM HEPES. Except where noted, all nanopore photochromic switching experiments

were performed on functionalized nanopores that had been removed from their Teflon housing and immersed in acetonitrile. All current measurements were conducted in the dark. More detailed descriptions of experimental methods and materials are provided in the supporting information and in earlier sources.^{24, 55}

ASSOCIATED CONTENT

The supporting information is available free of charge.

Experimental details including materials and methods; experimental and computational characterizations of the photoswitch; nanopore control experiments and characterizations (PDF)

The authors declare no competing financial interest.

AUTHOR INFORMATION

Corresponding Author

*Email: gracehan@brandeis.edu, jason dwyer@uri.edu

Author Contributions

The manuscript was written through contributions of all authors. All authors have given approval to the final version of the manuscript.

Funding Sources

This research has been supported by NSF award CHE-1808344 (JRD), and NIH award NIH 5R21HG011096 (JRD).

ACKNOWLEDGMENT

We thank Brian S. Sheetz for assistance with the measurement of nanopore conductance as a function of pH.

REFERENCES

- (1) Fried, J. P.; Swett, J. L.; Nadappuram, B. P.; Mol, J. A.; Edel, J. B.; Ivanov, A. P.; Yates, J. R. *In Situ* Solid-State Nanopore Fabrication. *Chem. Soc. Rev.* **2021**, *50*, 4974-4992, 10.1039/D0CS00924E. DOI: 10.1039/D0CS00924E.
- (2) Xue, L.; Yamazaki, H.; Ren, R.; Wanunu, M.; Ivanov, A. P.; Edel, J. B. Solid-State Nanopore Sensors. *Nature Reviews Materials* **2020**, *5*, 931-951. DOI: 10.1038/s41578-020-0229-6.
- (3) Pérez-Mitta, G.; Toimil-Molares, M. E.; Trautmann, C.; Marmisollé, W. A.; Azzaroni, O. Molecular Design of Solid-State Nanopores: Fundamental Concepts and Applications. *Adv. Mater.* **2019**, *31*, 1901483. DOI: https://doi.org/10.1002/adma.201901483.
- (4) Shi, W.; Friedman, A. K.; Baker, L. A. Nanopore Sensing. *Anal. Chem.* **2017**, *89*, 157-188. DOI: 10.1021/acs.analchem.6b04260.
- (5) Hagan, J. T.; Sheetz, B. S.; Bandara, Y. M. N. D. Y.; Karawdeniya, B. I.; Morris, M. A.; Chevalier, R. B.; Dwyer, J. R. Chemically Tailoring Nanopores for Single-Molecule Sensing and Glycomics. *Anal Bioanal Chem* **2020**, *412*, 6639-6654. DOI: 10.1007/s00216-020-02717-2.
- (6) Wang, J.; Zhou, Y.; Jiang, L. Bio-Inspired Track-Etched Polymeric Nanochannels: Steady-State Biosensors for Detection of Analytes. *ACS Nano* **2021**, *15*, 18974-19013. DOI: 10.1021/acsnano.1c08582.
- (7) Quick, J.; Loman, N. J.; Duraffour, S.; Simpson, J. T.; Severi, E.; Cowley, L.; Bore, J. A.; Koundouno, R.; Dudas, G.; Mikhail, A.; Ouédraogo, N.; Afrough, B.; Bah, A.; Baum, J. H. J.; Becker-Ziaja, B.; Boettcher, J. P.; Cabeza-Cabrerizo, M.; Camino-Sánchez, Á.; Carter, L. L.; Doerrbecker, J.; et al. Real-Time, Portable Genome Sequencing for Ebola Surveillance. *Nature* **2016**, *530*, 228. DOI: 10.1038/nature16996.
- (8) Ying, Y.-L.; Li, Z.-Y.; Hu, Z.-L.; Zhang, J.; Meng, F.-N.; Cao, C.; Long, Y.-T.; Tian, H. A Time-Resolved Single-Molecular Train Based on Aerolysin Nanopore. *Chem* **2018**, *4*, 1893-1901. DOI: https://doi.org/10.1016/j.chempr.2018.05.004.
- (9) Hu, Z.-L.; Li, Z.-Y.; Ying, Y.-L.; Zhang, J.; Cao, C.; Long, Y.-T.; Tian, H. Real-Time and Accurate Identification of Single Oligonucleotide Photoisomers Via an Aerolysin Nanopore. *Analytical Chemistry* **2018**, *90*, 4268-4272. DOI: 10.1021/acs.analchem.8b00096.
- (10) Zhang, X.; Zhang, J.; Ying, Y.-L.; Tian, H.; Long, Y.-T. Single Molecule Analysis of Light-Regulated Rna:Spiropyran Interactions. *Chemical Science* **2014**, *5*, 2642-2646, 10.1039/C4SC00134F. DOI: 10.1039/C4SC00134F.
- (11) Meng, F.-N.; Li, Z.-Y.; Ying, Y.-L.; Liu, S.-C.; Zhang, J.; Long, Y.-T. Structural Stability of the Photo-Responsive DNA Duplexes Containing One Azobenzene Via a Confined Pore. *Chemical Communications* **2017**, *53*, 9462-9465, 10.1039/C7CC04599A. DOI: 10.1039/C7CC04599A.
- (12) Klajn, R. Spiropyran-Based Dynamic Materials. *Chem Soc Rev* **2014**, *43*, 148-184. DOI: 10.1039/c3cs60181a.
- (13) Kortekaas, L.; Browne, W. R. The Evolution of Spiropyran: Fundamentals and Progress of an Extraordinarily Versatile Photochrome. *Chem Soc Rev* **2019**, *48*, 3406-3424. DOI: 10.1039/c9cs00203k.
- (14) Aprahamian, I. Hydrazone Switches and Things in Between. *Chem Commun* **2017**, *53*, 6674-6684. DOI: 10.1039/c7cc02879b.
- (15) Lerch, M. M.; Szymanski, W.; Feringa, B. L. The (Photo)Chemistry of Stenhouse Photoswitches: Guiding Principles and System Design. *Chem Soc Rev* **2018**, *47*, 1910-1937. DOI: 10.1039/c7cs00772h.

- (16) Villaron, D.; Wezenberg, S. J. Stiff-Stilbene Photoswitches: From Fundamental Studies to Emergent Applications. *Angew Chem Int Ed Engl* **2020**, *59*, 13192-13202. DOI: 10.1002/anie.202001031.
- (17) Mahimwalla, Z.; Yager, K. G.; Mamiya, J.-i.; Shishido, A.; Priimagi, A.; Barrett, C. J. Azobenzene Photomechanics: Prospects and Potential Applications. *Polymer Bulletin* **2012**, *69*, 967-1006. DOI: 10.1007/s00289-012-0792-0.
- (18) Dong, L.; Feng, Y.; Wang, L.; Feng, W. Azobenzene-Based Solar Thermal Fuels: Design, Properties, and Applications. *Chem Soc Rev* **2018**, *47*, 7339-7368. DOI: 10.1039/c8cs00470f.
- (19) D. Y. Bandara, Y. M. N.; Saharia, J.; Karawdeniya, B. I.; Hagan, J. T.; Dwyer, J. R.; Kim, M. J. Beyond Nanopore Sizing: Improving Solid-State Single-Molecule Sensing Performance, Lifetime, and Analyte Scope for Omics by Targeting Surface Chemistry During Fabrication. *Nanotechnology* **2020**, *31*, 335707. DOI: 10.1088/1361-6528/ab8f4d.
- (20) Bandara, Y. M. N. D. Y.; Karawdeniya, B. I.; Hagan, J. T.; Chevalier, R. B.; Dwyer, J. R. Chemically Functionalizing Controlled Dielectric Breakdown Silicon Nitride Nanopores by Direct Photohydrosilylation. *ACS Appl. Mater. Interfaces* **2019**, *11*, 30411-30420. DOI: 10.1021/acsami.9b08004.
- (21) Eggenberger, O. M.; Ying, C.; Mayer, M. Surface Coatings for Solid-State Nanopores. *Nanoscale* **2019**, *11*, 19636-19657, 10.1039/C9NR05367K. DOI: 10.1039/C9NR05367K. (22) Cayón, V. M.; Laucirica, G.; Toum Terrones, Y.; Cortez, M. L.; Pérez-Mitta, G.; Shen, J.; Hess, C.; Toimil-Molares, M. E.; Trautmann, C.; Marmisollé, W. A.; Azzaroni, O. Borate-Driven Ionic Rectifiers Based on Sugar-Bearing Single Nanochannels. *Nanoscale* **2021**, *13*, 11232-11241, 10.1039/D0NR07733J. DOI: 10.1039/D0NR07733J.
- (23) Waugh, M.; Briggs, K.; Gunn, D.; Gibeault, M.; King, S.; Ingram, Q.; Jimenez, A. M.; Berryman, S.; Lomovtsev, D.; Andrzejewski, L.; Tabard-Cossa, V. Solid-State Nanopore Fabrication by Automated Controlled Breakdown. *Nature Protocols* **2020**, *15*, 122-143. DOI: 10.1038/s41596-019-0255-2.
- (24) Karawdeniya, B. I.; Bandara, Y. M. N. D. Y.; Nichols, J. W.; Chevalier, R. B.; Dwyer, J. R. Surveying Silicon Nitride Nanopores for Glycomics and Heparin Quality Assurance. *Nat Commun* **2018**, *9*, 3278. DOI: 10.1038/s41467-018-05751-y.
- (25) García-Iriepa, C.; Marazzi, M.; Frutos, L. M.; Sampedro, D. E/Z Photochemical Switches: Syntheses, Properties and Applications. *RSC Advances* **2013**, *3*. DOI: 10.1039/c2ra22363e.
- (26) Liu, X.-M.; Jin, X.-Y.; Zhang, Z.-X.; Wang, J.; Bai, F.-Q. Theoretical Study on the Reaction Mechanism of the Thermal Cis—Trans Isomerization of Fluorine-Substituted Azobenzene Derivatives. *RSC Advances* **2018**, *8*, 11580-11588. DOI: 10.1039/c8ra01132j.
- (27) Qiu, Q.; Gerkman, M. A.; Shi, Y.; Han, G. G. D. Design of Phase-Transition Molecular Solar Thermal Energy Storage Compounds: Compact Molecules with High Energy Densities. *Chem Commun (Camb)* **2021**, *57*, 9458-9461. DOI: 10.1039/d1cc03742k.
- (28) Priimagi, A.; Shevchenko, A. Azopolymer-Based Micro- and Nanopatterning for Photonic Applications. *Journal of Polymer Science Part B: Polymer Physics* **2014**, *52*, 163-182. DOI: 10.1002/polb.23390.
- (29) Wu, S.; Butt, H. J. Solar-Thermal Energy Conversion and Storage Using Photoresponsive Azobenzene-Containing Polymers. *Macromol Rapid Commun* **2020**, *41*, e1900413. DOI: 10.1002/marc.201900413.
- (30) Ren, H.; Yang, P.; Winnik, F. M. Azopyridine: A Smart Photo- and Chemo-Responsive Substituent for Polymers and Supramolecular Assemblies. *Polymer Chemistry* **2020**, *11*, 5955-5961, 10.1039/D0PY01093F. DOI: 10.1039/D0PY01093F.

- (31) Shin, K.; Shin, E. J. Photoresponsive Azobenzene-Modified Gold Nanoparticle. *Bull. Korean Chem. Soc.* **2008**, *29*, 1259-1262. DOI: 10.5012/bkcs.2008.29.6.1259.
- (32) Klajn, R. Immobilized Azobenzenes for the Construction of Photoresponsive Materials. *Pure and Applied Chemistry* **2010**, *82*, 2247-2279. DOI: 10.1351/pac-con-10-09-04.
- (33) Zhao, T.; Chen, L.; Li, Q.; Li, X. Near-Infrared Light Triggered Drug Release from Mesoporous Silica Nanoparticles. *J Mater Chem B* **2018**, *6*, 7112-7121. DOI: 10.1039/c8tb01548a.
- (34) Jia, S.; Fong, W.-K.; Graham, B.; Boyd, B. J. Photoswitchable Molecules in Long-Wavelength Light-Responsive Drug Delivery: From Molecular Design to Applications. *Chemistry of Materials* **2018**, *30*, 2873-2887. DOI: 10.1021/acs.chemmater.8b00357.
- (35) Grommet, A. B.; Lee, L. M.; Klajn, R. Molecular Photoswitching in Confined Spaces. *Acc Chem Res* **2020**, *53*, 2600-2610. DOI: 10.1021/acs.accounts.0c00434.
- (36) Rivas, F.; Zahid, O. K.; Reesink, H. L.; Peal, B. T.; Nixon, A. J.; DeAngelis, P. L.; Skardal, A.; Rahbar, E.; Hall, A. R. Label-Free Analysis of Physiological Hyaluronan Size Distribution with a Solid-State Nanopore Sensor. *Nat Commun* **2018**, *9*, 1037. DOI: 10.1038/s41467-018-03439-x.
- (37) Ghavidast, A.; Mahmoodi, N. O. A Comparative Study of the Photochromic Compounds Incorporated on the Surface of Nanoparticles. *Journal of Molecular Liquids* **2016**, *216*, 552-564. DOI: 10.1016/j.molliq.2015.12.014.
- (38) Negishi, Y.; Kamimura, U.; Ide, M.; Hirayama, M. A Photoresponsive Au25 Nanocluster Protected by Azobenzene Derivative Thiolates. *Nanoscale* **2012**, *4*, 4263-4268. DOI: 10.1039/c2nr30830d.
- (39) Kowalczyk, S. W.; Grosberg, A. Y.; Rabin, Y.; Dekker, C. Modeling the Conductance and DNA Blockade of Solid-State Nanopores. *Nanotechnology* **2011**, *22*, 315101.
- (40) Wanunu, M.; Meller, A. Chemically Modified Solid-State Nanopores. *Nano Lett.* **2007**, *7*, 1580-1585. DOI: 10.1021/nl070462b.
- (41) Yusko, E. C.; Johnson, J. M.; Majd, S.; Prangkio, P.; Rollings, R. C.; Li, J.; Yang, J.; Mayer, M. Controlling Protein Translocation through Nanopores with Bio-Inspired Fluid Walls. *Nat Nanotechnol* **2011**, *6*, 253-260. DOI: 10.1038/nnano.2011.12.
- (42) Fu, K.; Bohn, P. W. Nanopore Electrochemistry: A Nexus for Molecular Control of Electron Transfer Reactions. *ACS Central Science* **2018**, *4*, 20-29. DOI: 10.1021/acscentsci.7b00576.
- (43) Grommet, A. B.; Feller, M.; Klajn, R. Chemical Reactivity under Nanoconfinement. *Nature Nanotechnology* **2020**, *15*, 256-271. DOI: 10.1038/s41565-020-0652-2.
- (44) Hoefnagel, M. A.; van Veen, A.; Wepster, B. M. Protonation of Azo-Compounds. Part Ii. The Structure of the Conjugate Acid of *Trans*-Azobenzene. *Rec. Trav. Chim. Pays-Bas* **1969**, *88*, 562-572. DOI: 10.1002/recl.19690880507.
- (45) Gibson, R. S. L.; Calbo, J.; Fuchter, M. J. Chemical Z E Isomer Switching of Arylazopyrazoles Using Acid. *ChemPhotoChem* **2019**, *3*, 372-377. DOI: 10.1002/cptc.201900065.
- (46) Groten, J.; Bunte, C.; Ruhe, J. Light-Induced Switching of Surfaces at Wetting Transitions through Photoisomerization of Polymer Monolayers. *Langmuir* **2012**, *28*, 15038-15046. DOI: 10.1021/la302764k.
- (47) Feng, N.; Han, G.; Dong, J.; Wu, H.; Zheng, Y.; Wang, G. Nanoparticle Assembly of a Photo- and Ph-Responsive Random Azobenzene Copolymer. *J Colloid Interface Sci* **2014**, *421*, 15-21. DOI: 10.1016/j.jcis.2014.01.036.

- (48) Weng, C.-H.; Lin, C.-C.; Tsai, F.-C.; Dai, C.-A.; Yang, F.-L.; Shih, W.-P.; Chang, P.-Z. Photo-Controllable Contact Angle Hysteresis on an Artificial Azo-Ipn Petal. *Materials Letters* **2018**, *219*, 81-84. DOI: 10.1016/j.matlet.2018.02.073.
- (49) Firnkes, M.; Pedone, D.; Knezevic, J.; Döblinger, M.; Rant, U. Electrically Facilitated Translocations of Proteins through Silicon Nitride Nanopores: Conjoint and Competitive Action of Diffusion, Electrophoresis, and Electroosmosis. *Nano Lett.* **2010**, *6*, 895-909, doi: 10.1021/nl100861c. DOI: 10.1021/nl100861c.
- (50) Kortekaas, L.; Simke, J.; Arndt, N. B.; Böckmann, M.; Doltsinis, N. L.; Ravoo, B. J. Acid-Catalysed Liquid-to-Solid Transitioning of Arylazoisoxazole Photoswitches. *Chemical Science* **2021**, *12*, 11338-11346. DOI: 10.1039/d1sc03308e.
- (51) Goulet-Hanssens, A.; Utecht, M.; Mutruc, D.; Titov, E.; Schwarz, J.; Grubert, L.; Bleger, D.; Saalfrank, P.; Hecht, S. Electrocatalytic Z --> E Isomerization of Azobenzenes. *J Am Chem Soc* **2017**, *139*, 335-341. DOI: 10.1021/jacs.6b10822.
- (52) Yasuda, H.; Buskohl, P. R.; Gillman, A.; Murphey, T. D.; Stepney, S.; Vaia, R. A.; Raney, J. R. Mechanical Computing. *Nature* **2021**, *598*, 39-48. DOI: 10.1038/s41586-021-03623-y.
- (53) Chen, K.; Zhu, J.; Bošković, F.; Keyser, U. F. Nanopore-Based DNA Hard Drives for Rewritable and Secure Data Storage. *Nano Letters* **2020**, *20*, 3754-3760. DOI: 10.1021/acs.nanolett.0c00755.
- (54) Rutten, M. G. T. A.; Vaandrager, F. W.; Elemans, J. A. A. W.; Nolte, R. J. M. Encoding Information into Polymers. *Nature Reviews Chemistry* **2018**, *2*, 365-381. DOI: 10.1038/s41570-018-0051-5.
- (55) Xia, K.; Hagan, J. T.; Fu, L.; Sheetz, B. S.; Bhattacharya, S.; Zhang, F.; Dwyer, J. R.; Linhardt, R. J. Synthetic Heparan Sulfate Standards and Machine Learning Facilitate the Development of Solid-State Nanopore Analysis. *P Natl Acad Sci USA* **2021**, *118*, e2022806118. DOI: 10.1073/pnas.2022806118.
- (56) Anderson, B. N.; Muthukumar, M.; Meller, A. Ph Tuning of DNA Translocation Time through Organically Functionalized Nanopores. *ACS Nano* **2013**, *7*, 1408-1414, doi: 10.1021/nn3051677. DOI: 10.1021/nn3051677 (accessed 2013/06/12).
- (57) Ando, G.; Hyun, C.; Li, J.; Mitsui, T. Directly Observing the Motion of DNA Molecules near Solid-State Nanopores. *ACS Nano* **2012**, *6*, 10090-10097, doi: 10.1021/nn303816w. DOI: 10.1021/nn303816w (accessed 2013/02/18).
- (58) Matsui, M.; Funabiki, K.; Shibata, K. Synthesis and Uv/Vis Absorption Spectra of Novel Azo Dyes Derived from Polyfluoro- and Perfluoroazobenzenes. *Bull. Chem. Soc. Jpn.* **2002**, *75*, 531-536. DOI: 10.1246/bcsj.75.531.
- (59) You, F.; Paik, M. Y.; Häckel, M.; Kador, L.; Kropp, D.; Schmidt, H. W.; Ober, C. K. Control and Suppression of Surface Relief Gratings in Liquid-Crystalline Perfluoroalkyl—Azobenzene Polymers. *Advanced Functional Materials* **2006**, *16*, 1577-1581. DOI: 10.1002/adfm.200500711.
- (60) Arima, H.; Saito, T.; Kajitani, T.; Yagai, S. Self-Assembly of Alkylated and Perfluoroalkylated Scissor-Shaped Azobenzene Dyads into Distinct Structures. *Chem Commun (Camb)* **2020**, *56*, 15619-15622. DOI: 10.1039/d0cc06907h.
- (61) Kwok, H.; Briggs, K.; Tabard-Cossa, V. Nanopore Fabrication by Controlled Dielectric Breakdown. *PLoS ONE* **2014**, *9*, e92880. DOI: 10.1371/journal.pone.0092880.
- (62) Dassault Systèmes. *Biovia Discovery Studio Visualizer*; Dassault Systèmes: San Diego, 2019.

(63) Frisch, M. J.; Truck, G. W.; Schlegel, H. B.; Scuseria, G. E.; Robb, M. A.; Cheeseman, J. R.; Scalmani, G.; Barone, B.; Mennucci, B.; Petersson, G. A.; Nakatsuji, H.; Caricato, M.; Li, X.; Hratchian, H. P.; Izmaylov, A. F.; Bloino, J.; Zheng, G.; Sonnenberg, J. L.; Hada, M.; Ehara, M.; et al. Gaussian 09; Gaussian, Inc.: Wallingford CT, 2009.

(64) Tabard-Cossa, V.; Trivedi, D.; Wiggin, M.; Jetha, N. N.; Marziali, A. Noise Analysis and Reduction in Solid-State Nanopores. *Nanotechnology* 2007, *18*. DOI: http://dx.doi.org/10.1088/0957-4484/18/30/305505.

SUPPORTING INFORMATION

Photoswitchable Binary Nanopore Conductance and Selective Electronic Detection of Single Biomolecules Under Wavelength and Voltage Polarity Control

James T. Hagan¹, Alejandra Gonzalez², Yuran Shi², Grace G.D. Han²*, and Jason R. Dwyer¹*

1. Department of Chemistry, University of Rhode Island, 140 Flagg Rd., Kingston, RI, 02881.

2. Department of Chemistry, Brandeis University, 415 South Street, Waltham, Massachusetts

Table of Contents

02453, United States

Nanopore-Centric Experimental Details	. 28
Azobenzene-Specific Experimental Details	. 30
Supporting Information Figures	. 32

Nanopore-Centric Experimental Details Commercial Materials

For nanopore experiments HEPES potassium salt (H0527, ≥99.5% (titration)), potassium chloride (60130, puriss. p. a., ≥99.5% (AT)), potassium hydroxide (306568, 99.99%), hydrochloric acid (320331, ACS reagents, 37%), acetonitrile (34998, ≥99.9), and maltodextrin (419680, dextrose equivalent 13-17) were purchased from Millipore-Sigma Corporation (Burlington, MA, USA) and used without further purification. NoLimits 3 kbp dsDNA fragment solutions were purchased from ThermoFisher Scientific (SM1711). Anhydrous ethanol (111000200, 100%) was purchased from Pharmco (Brookfield, CT, USA) and used without further purification.

All electrolyte solutions were prepared using Type I water (SYNSVHFUS, ~18 MΩ·cm resistivity, Millipore Synergy UV, Billerica, MA, USA)) and passed through a Stericup Quick Release vacuum filter system (S2GPU10RE, 0.22 μm pore polyethersulfone filter membrane, EMD Millipore Corporation, MA, USA). The electrolyte solutions were buffered with 10 mM HEPES and adjusted to pH 7 by adding concentrated HCl and KOH solutions dropwise as needed. All other aqueous solutions used in this work was sourced from the type I water filter.

Nanopore Fabrication and Characterization

A detailed accounting of the nanopore apparatus is described in previous work.²⁴ Isolated nanopores were formed by controlled dielectric breakdown as described previously.^{23, 24, 61} We used15±2 nm-thick LPCVD silicon nitride (SiN_x) membranes supported on 200 μm-thick silicon frames (NBPT005Z-HR, Lot # L03203-01) purchased from Norcada, Inc. (Edmonton, AB, Canada). In brief, ~10 V was applied across the free-standing SiN_x membrane immersed in 1 M KCl buffered to pH 7 in 10 mM HEPES. The resulting nanopore was characterized by its conductance, which was calculated by a linear fit to its Ohmic current-voltage curve from -200 to

200 mV. Nanopore conductance measurements were made at an acquisition rate of 10 kHz using a 1 kHz Bessel filter.

Nanopore Photohydrosilylation

The general method for photohydrosilylation of SiN_x nanopores has been detailed previously.²⁰ A small amount (~5 to 10 mg) of the azo switch in all *trans* configuration (confirmed by NMR) was moved to a 12 mL borosilicate glass sample vial (14-955-310, Fisher Scientific, Waltham, MA, USA). A minimum of acetonitrile was used to dissolve the solid. A membrane chip with a freshly formed SiN_x nanopore was rinsed with water, then ethanol, and then taken out of the PTFE housing before being mounted in a custom aluminum reaction chamber, covered with the azobenzene solution, and irradiated under a mercury UV lamp (95-0042-05, Mineralight XX-15S, UVP, Upland, CA, USA) for at least 3 hours.²⁰ The chip was then rinsed in ethanol and placed back into the PTFE fluid cell. This was filled with ethanol, then water, and then the 1 M KCl electrolyte solution buffered at pH 7 (10 mM HEPES). The nanopore conductance was then measured and this measurement is labelled "initial".

Nanopore Photoswitching

Switching was achieved by irradiating the membrane with either white (FLE23HT3/2/SW, GE, NYC, NY, USA) or UV light (SV003 10 W 365 nm UV flashlight, Alonefire, China) to convert the azobenzene to its *trans* or *cis* configuration, respectively. The membrane was rinsed in its PTFE holder by exchanging the electrolyte with water and then ethanol before removing it from the holder and placing it in the aluminum reaction chamber. The membrane was then covered with acetonitrile and irradiated under the relevant light source while shielded from ambient light. After desired irradiation time, the membrane was remounted and characterized by conductance in the PTFE holder as described above.

Nanopore Sensing Conditions

All constant voltage nanopore experiments (current *versus* time measurements) were run using a 1 M KCl solution buffered to pH 7 with 10 mM HEPES. Measurements were collected over 10 to 20 minutes using a Molecular Devices Axopatch 200B with an acquisition rate of 100 kHz and 10 kHz Bessel filter. The open-pore baseline current was checked for steadiness under a potential of +200 mV and -200 mV before adding analyte to the flow cell. For maltodextrin experiments, 10 μL of a 2 mg/mL stock solution (0.2% w/v) was added to the ground side of the flow cell, resulting in a sensing concentration of ~0.04 mg/mL (0.004% w/v). For 3 kbp DNA experiments, 10 μL of the 0.5 mg/mL stock solution was added to the ground side, resulting in a sensing concentration of ~0.01 mg/mL.

Nanopore Signal Analysis

Raw nanopore current traces were analyzed using custom algorithms written in Python 3.8 and described in more detail previously.⁵⁵ In brief, conductance traces were segmented into 1-200 ms windows for computational tractability. Events (when present) within each window were then isolated by thresholding.

Azobenzene-Specific Experimental Details

For synthesis of 4-(propargyloxy)azobenzene, 4-phenylazophenol (B25198, 98%) was purchased from Alfa Aesar (Tewksbury, MA, USA) and used without further purification. Propargyl bromide (81830, 97%) was purchased from Fluka (now Honeywell [Charlotte, NC]) and used without further purification. Anhydrous potassium carbonate (P208-500, ≥99.0%) was purchased from Fisher Chemical (Waltham, MA, USA) and used without further purification. Acetone (A18-4, Certified ACS) was purchased from Fisher Chemical (Waltham, MA, USA) and

dried overnight with 3 Å molecular sieves (L05335, 1-2 mm, 0.04-0.08 in beads) purchased from Alfa Aesar (Tewksbury, MA, USA).

For UV-Vis experiments, HEPES potassium salt (H0527, ≥99.5% (titration)) was purchased from Millipore-Sigma Corporation (Burlington, MA, USA) and used without further purification. Potassium chloride (BP366-500, >99%), hydrochloric acid (A144-212, Certified ACS Plus, 36.5 to 38.0%), and acetonitrile (A998-4, ≥99.9%) was purchased from Fisher Chemical (Waltham, MA, USA) and used without further purification. Aqueous solutions were prepared as described above using Type I water (~18 MΩ·cm resistivity, Elga PURELAB Flex 2, Woodridge, IL, USA) and passed through a Stericup Quick Release vacuum filter system (S2GPU10RE, 0.22 μm pore polyethersulfone filter membrane, EMD Millipore Corporation, MA, USA). Samples were irradiated with white light, a 275 nm wavelength LED (M275L4, 45 mW, 700 mA), a 365 nm wavelength LED (M365LP1, 1350 mW, 1700 mA), or 430 nm wavelength LED (M430L4, 490 mW, 500 mA). LEDs were purchased from Thorlabs (Newton, NJ). UV-Vis experiments were run using a Varian Cary 50 Bio UV-Visible Spectrophotometer.

Procedure for synthesis of 4-(propargyloxy)azobenzene

4-azophenol (1.982 g, 10 mmol), potassium carbonate (6.910 g, 50 mmol, 5 eq.), and anhydrous acetone (120 mL) were added to a flask and stirred for 30 minutes at room temperature under argon. Then, a solution of propargyl bromide (3.79 mL, 50 mmol, 5 eq.) in acetone (16.2 mL) was added dropwise to the reaction mixture. The reaction was left to stir for 33 hours under argon. Upon completion of the reaction, solvent was removed under reduced pressure and the product was obtained by column chromatography (9:1 hexanes: diethyl ether to 4:1 hexanes: diethyl ether) as an orange solid (1.289 g, 5.45 mmol, 54.5%). ¹H NMR (CDC13, 400 MHz) 7.94 (d, 2H), 7.88 (d, 2H), 7.51 (t, 2H), 7.45 (t, 1H), 7.10 (d, 1H), 4.78 (d, 2H), 2.57 (t, 1H).

Supporting Information Figures

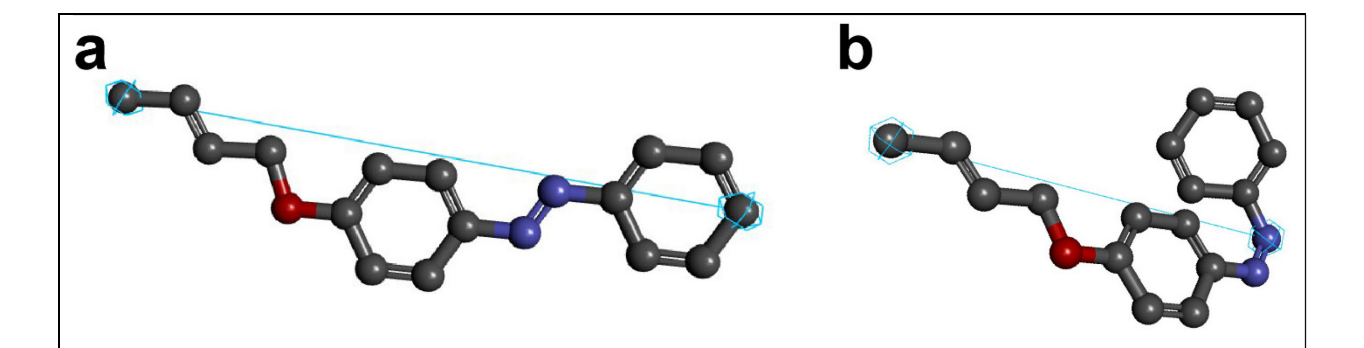


Figure S1. a) *trans*-azobenzene 1.47 nm distance from anchor to surface-distal terminus point; b) *cis*-azobenzene 1.05 nm distance from anchor to surface-distal terminus point. These two distances are used as the presumed thickness of a monolayer of each configuration. Both *cis* and *trans* structures were modeled using BIOVIA Discovery Studio Visualizer.⁶²

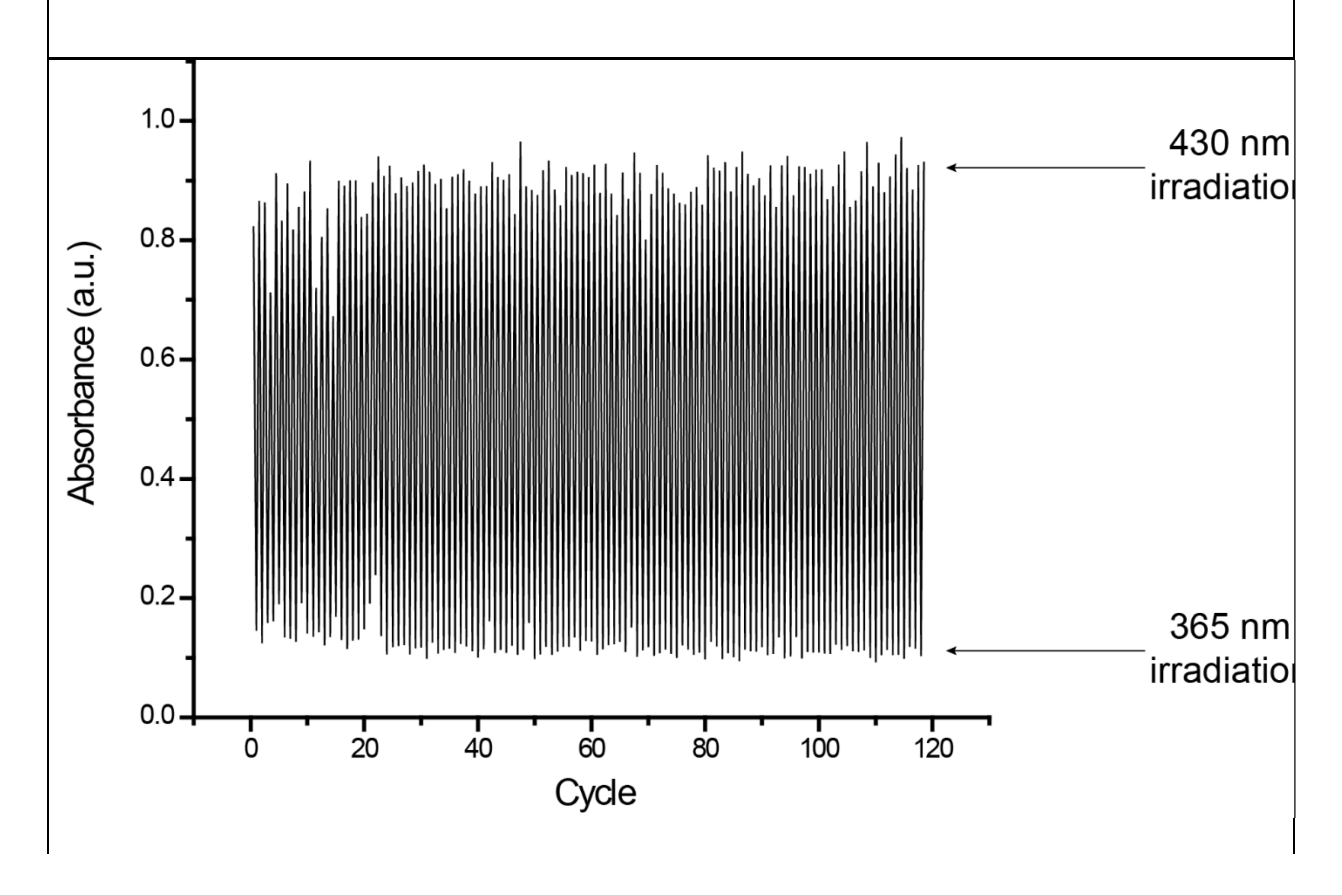


Figure S2. The absorbance change of 4-(propargyloxy)azobenzene monitored at 338 nm (the peak wavelength of the π - π * absorption band of the E isomer) during cycling between e cis-rich (365 nm) and e trans-rich (430 nm) states in acetonitrile. Each cycle was recorded after 15 seconds of irradiation.

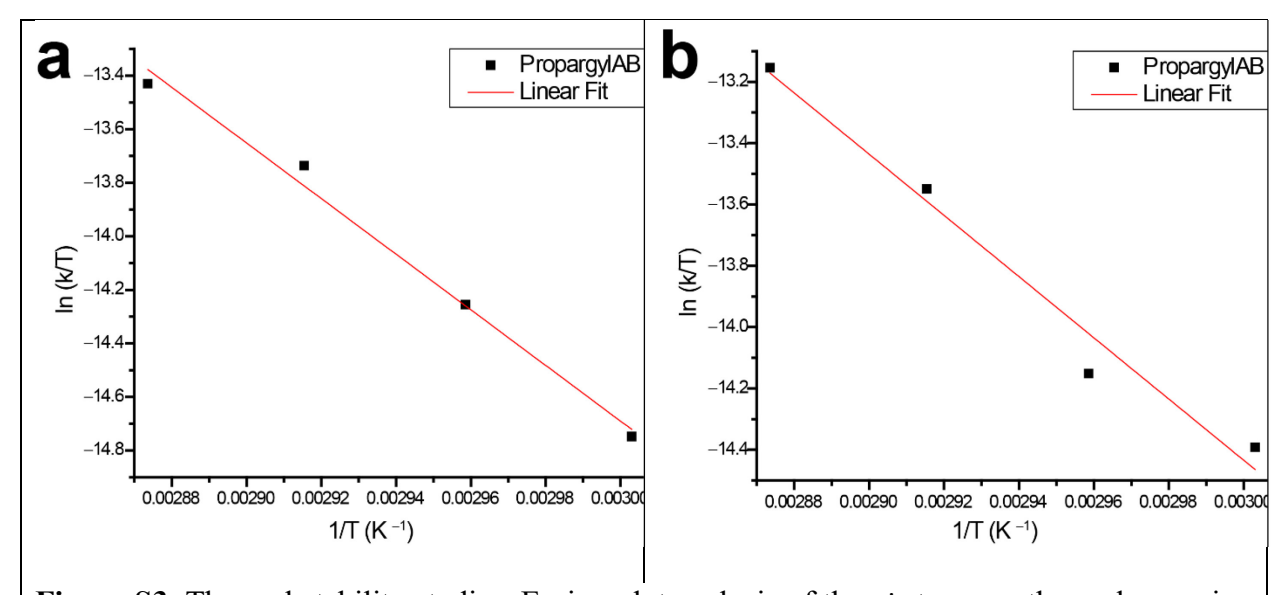


Figure S3. Thermal stability studies. Eyring plot analysis of the *cis*-to-*trans* thermal reversion of 4-(propargyloxy)azobenzene monitored in (a) acetonitrile at 60, 65, and 70, and 75°C: $\Delta H \ddagger = 86 \text{ kJ/mol}$; $\Delta S \ddagger = -61 \text{ J/(mol \cdot K)}$ so that at 298.15 K, $\Delta G = 104.5 \text{ kJ/mol}$, $t_{1/2} = \ln 2/k = 61 \text{ h}$, and (b) 1M KCl/10 mM HEPES solution at 60, 65, 70, and 75°C: $\Delta H \ddagger = 83 \text{ kJ/mol}$; $\Delta S \ddagger = -68 \text{ J/(mol \cdot K)}$ so that at 298.15K, $\Delta G = 103.4 \text{ kJ/mol}$, $t_{1/2} = \ln 2/k = 41 \text{ h}$

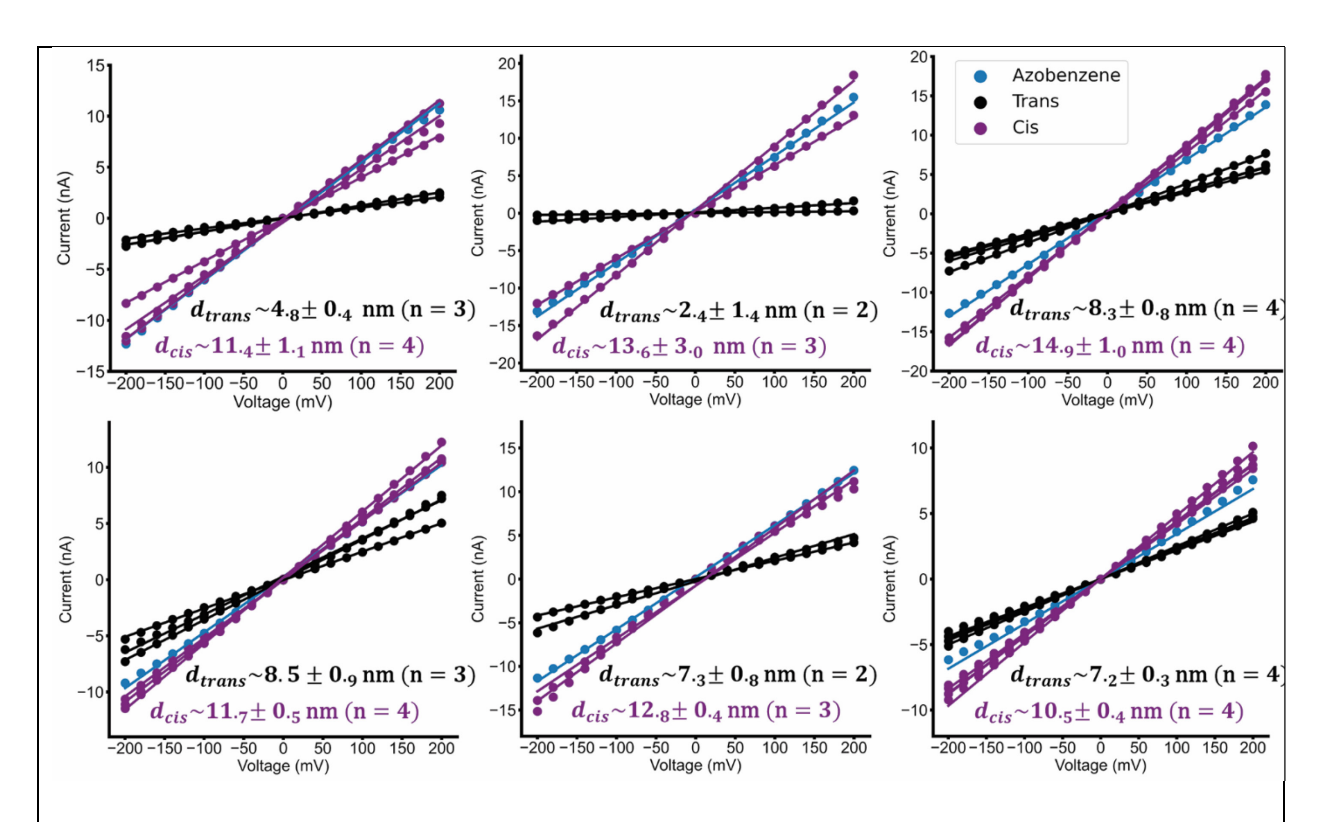
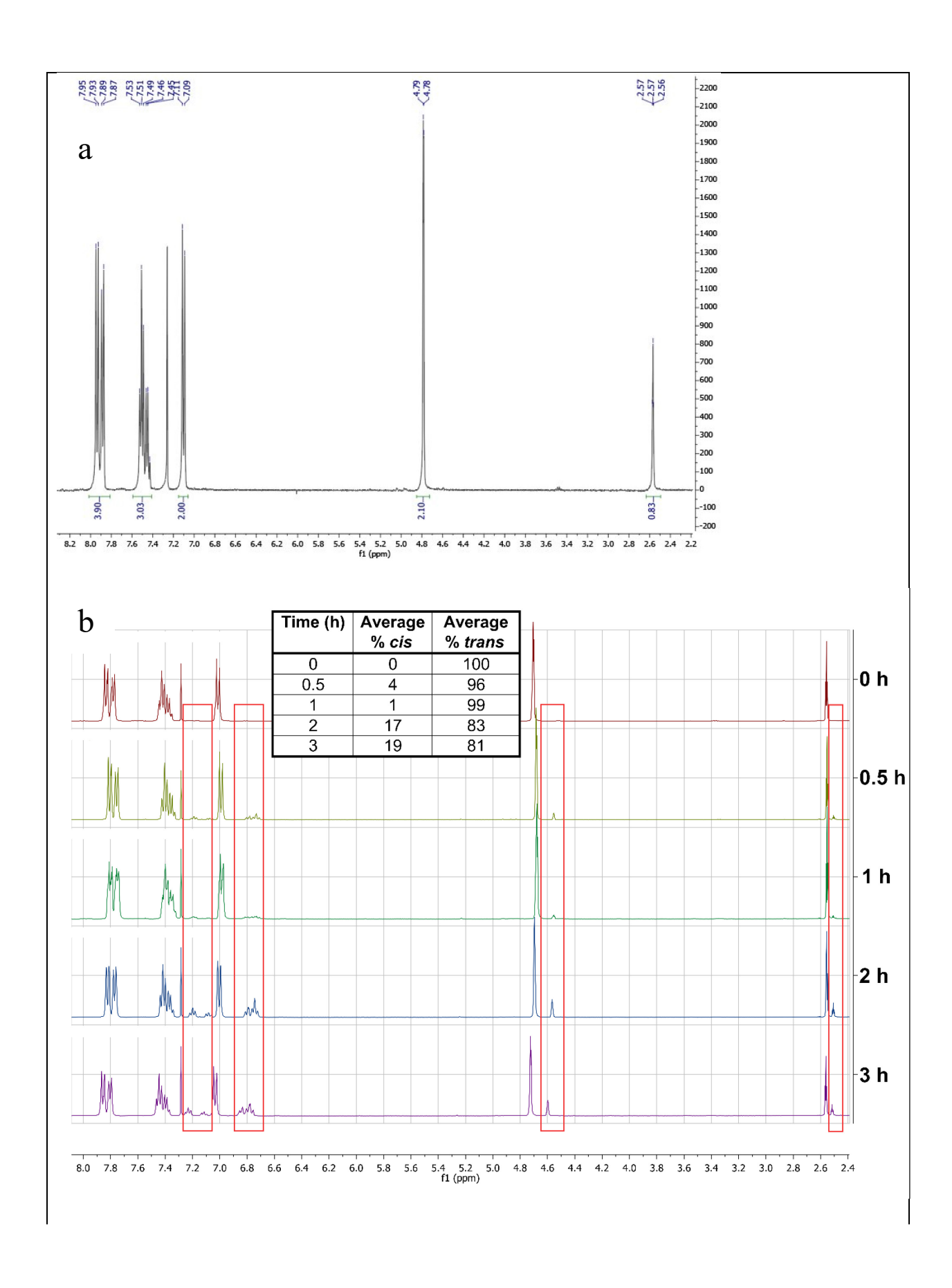


Figure S4. Each independent functionalized pore was photoswitched several times. Before and after each trial, an IV curve was collected in 1 M KCl buffered to pH 7 by 10 mM HEPES to characterize any resulting change in the pore's conductance. Switching was done with the pore submerged in acetonitrile using either a white light or a UV LED flashlight.



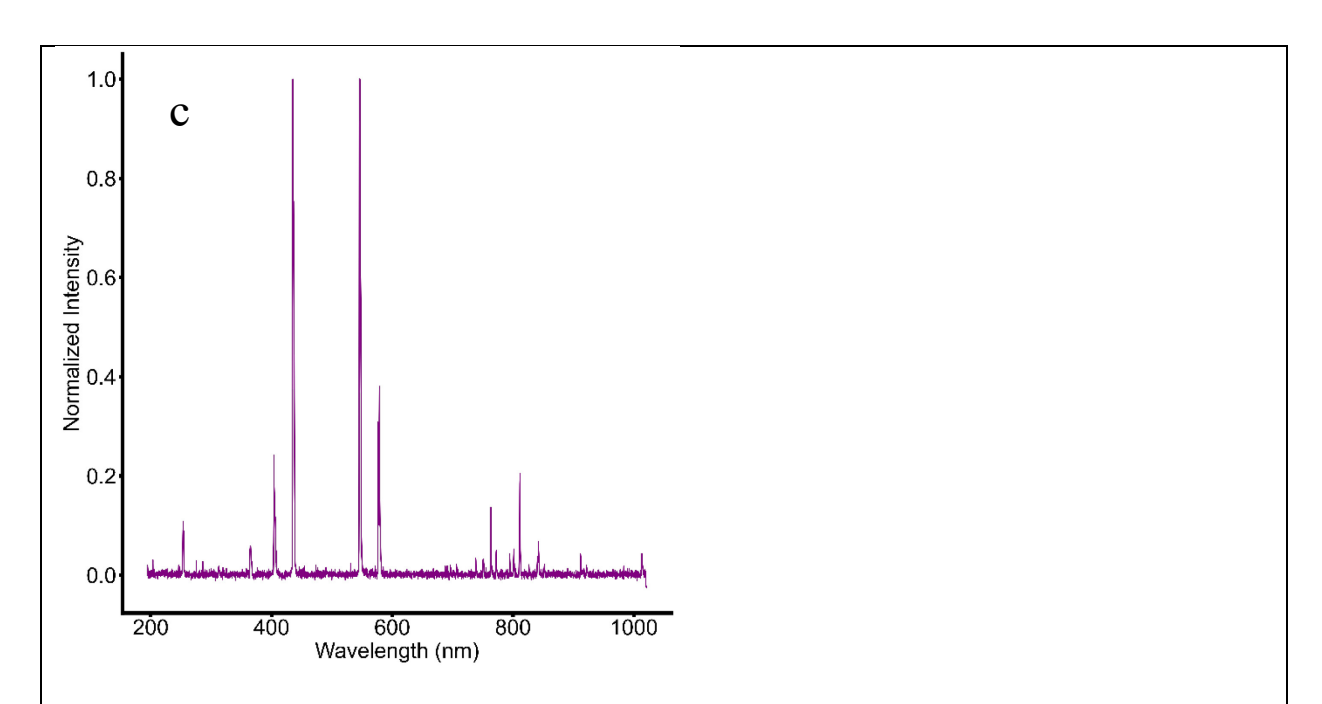
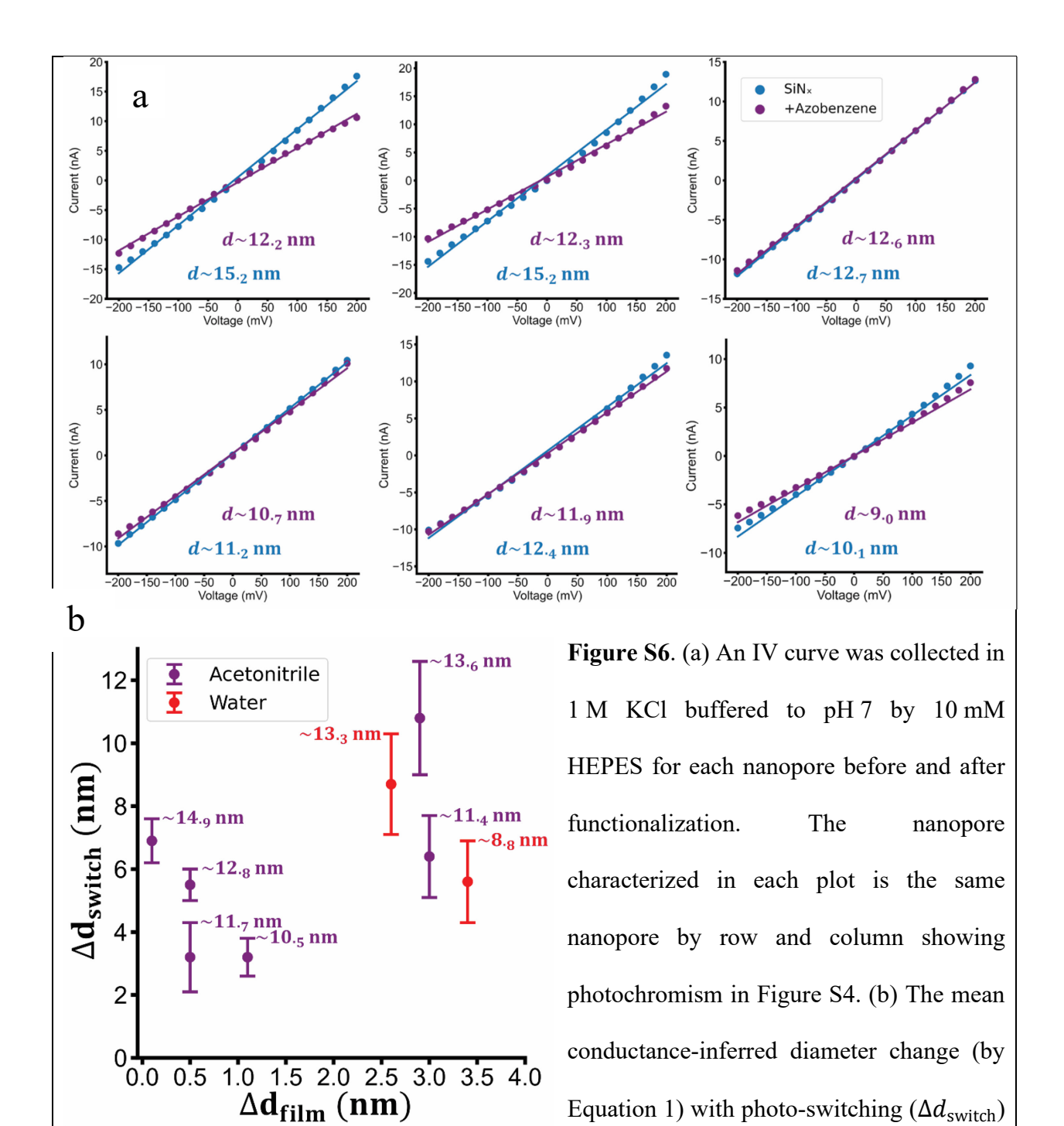


Figure S5. NMR spectra for the (a) as-synthesized *trans*-4-(propargyloxy)azobenzene and (b) molecule in bulk acetonitrile solution under photohydrosilylation irradiation conditions. In (b), aliquots of the originally *trans* azobenzene (~55 mM) were collected at the time intervals listed from a solution otherwise continuously irradiated in a quartz cuvette using the mercury UV lamp. No decomposition products of this molecule were detected but an overall conversion from a purely *trans* to a mixed *cis/trans* (19%/81%) sample in bulk solution was evident. The UV/Vis spectrum of the mercury lamp used for photohydrosilylation is shown in (c).



from Figure S4 is plotted against the change in nanopore diameter after coating ($\Delta d_{\rm film}$) in (a) to show the degree to which the two diameter changes were correlated. The values next to each data point are the mean nanopore diameters of the *cis*-state of the nanopore in Figure S4. The

 Δd_{film} for the two pores switched in pure water were used with the six pores in (a) in calculating the mean Δd_{film} reported in the main manuscript.

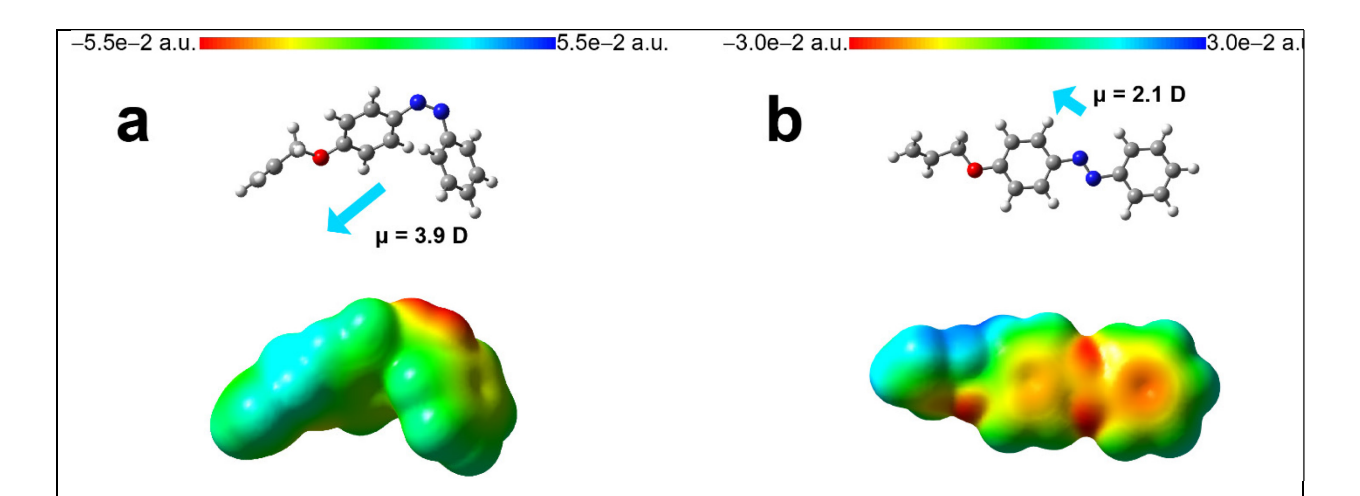


Figure S7. Atomic models and electrostatic maps of the 4-(propargyloxy)azobenzene in (a) *cis* and (b) *trans* configurations. The relative size of dipole moment is expressed as the length of arrows. The structures and electrostatic potential maps of both *cis* and *trans* isomers of 4-(propargyloxy)azobenzene were calculated using density functional theory (DFT)/B3LYP method with a 6-31G (d,p) basis set. DFT calculations were performed with the Gaussian 09 program.⁶³

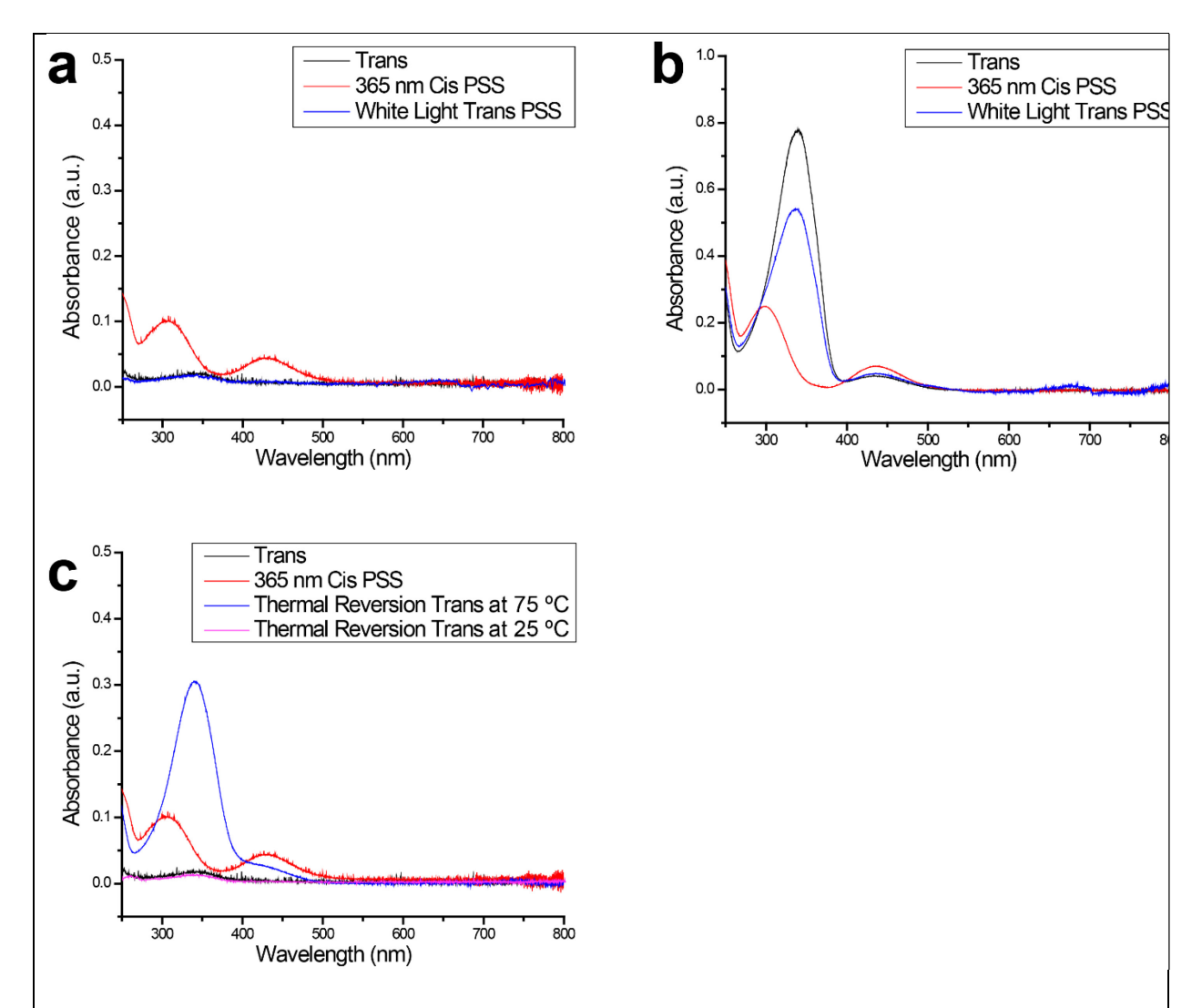


Figure S8. UV-Vis absorption spectra of 4-(propargyloxy)azobenzene at the photostationary state under irradiation (beginning with the *trans* isomer) at the indicated wavelengths at 25°C in (a) 1 M KCl/10 mM HEPES solution and (b) acetonitrile. (c) UV-Vis absorption spectra of 4-(propargyloxy) azobenzene in 1 M KCl/10 mM HEPES solution at the photostationary state under irradiation at 365 nm, upon thermal reversion at 75°C, and upon cooling to 25°C. In (a), it took about 15 minutes for the *cis* isomer to reach the photostationary state under 365 nm irradiation, and about 90 minutes to reach the *trans* photostationary state with white light irradiation. In (b), it took about 15 minutes for the *cis* isomer to reach the photostationary state

under 365 nm irradiation, and about 90 minutes to reach the *trans* photostationary state under white light irradiation. In (c), it took about 10 minutes for the *cis* isomer to reach the photostationary state under 365 nm irradiation, and about 85 minutes for the *cis* compound to thermally revert to the *trans* isomer upon heating at 75°C. The *trans* isomer was soluble in the aqueous solution at the high temperature and precipitated upon cooling to 25°C.

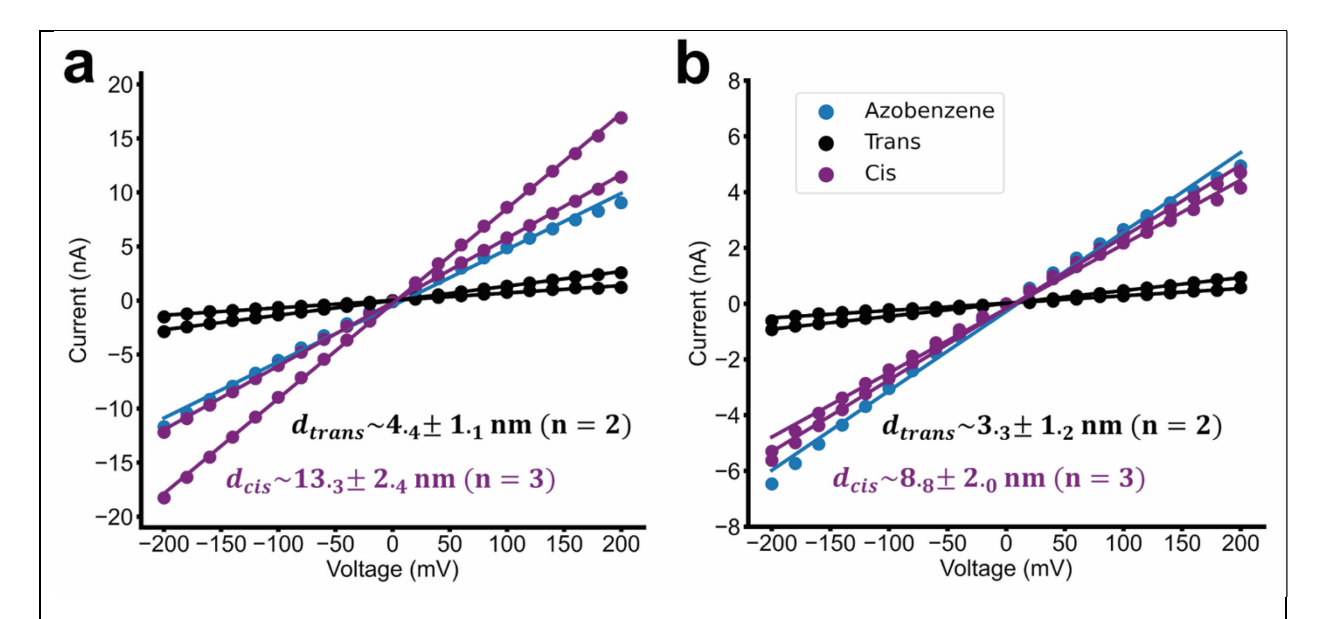


Figure S9. Switching of the (a) 13.5 and (b) 9 nm diameter nanopores in ultrapure water, demonstrating the potential for *in situ* switching without removing the nanopore membrane from the fluidic cell. The IV curves were collected in 1 M KCl buffered at pH 7 with 10 mM HEPES.

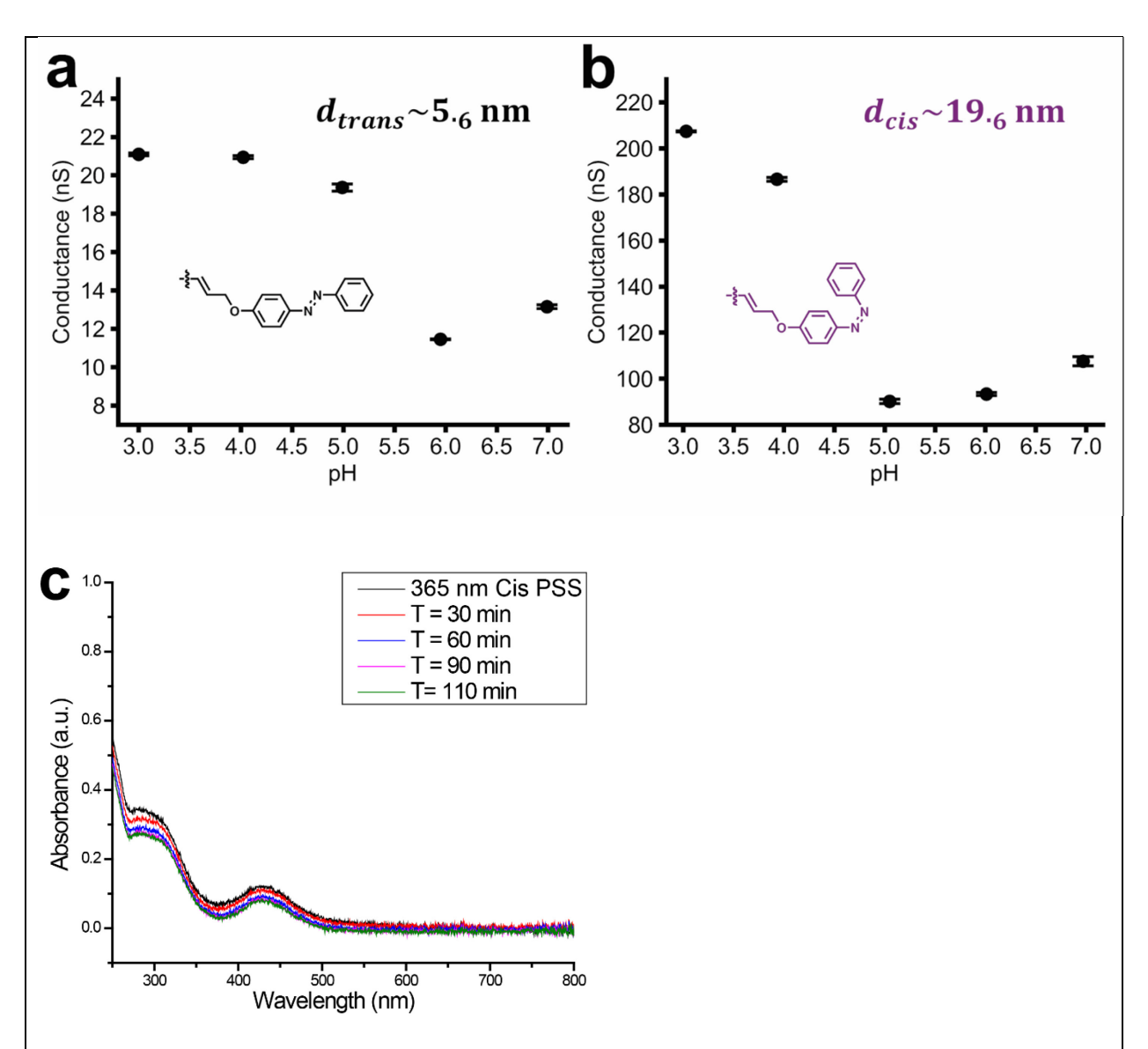


Figure S10. A conductance (G) vs pH curve for the same nanopore in the (a) *trans* and (b) *cis* configuration collected in 1 M KCl and 10 mM HEPES, with pH swept from acidic to basic values. (c) UV-Vis absorption spectra of 4-(propargyloxy) azobenzene in 1 M KCl/10 mM HEPES solution set to pH 3 and initially at the photostationary state under UV (365 nm) at 25°C. Time points over a 110-minute period show that the compound undergoes minimal thermal reversion back to the *trans* isomer

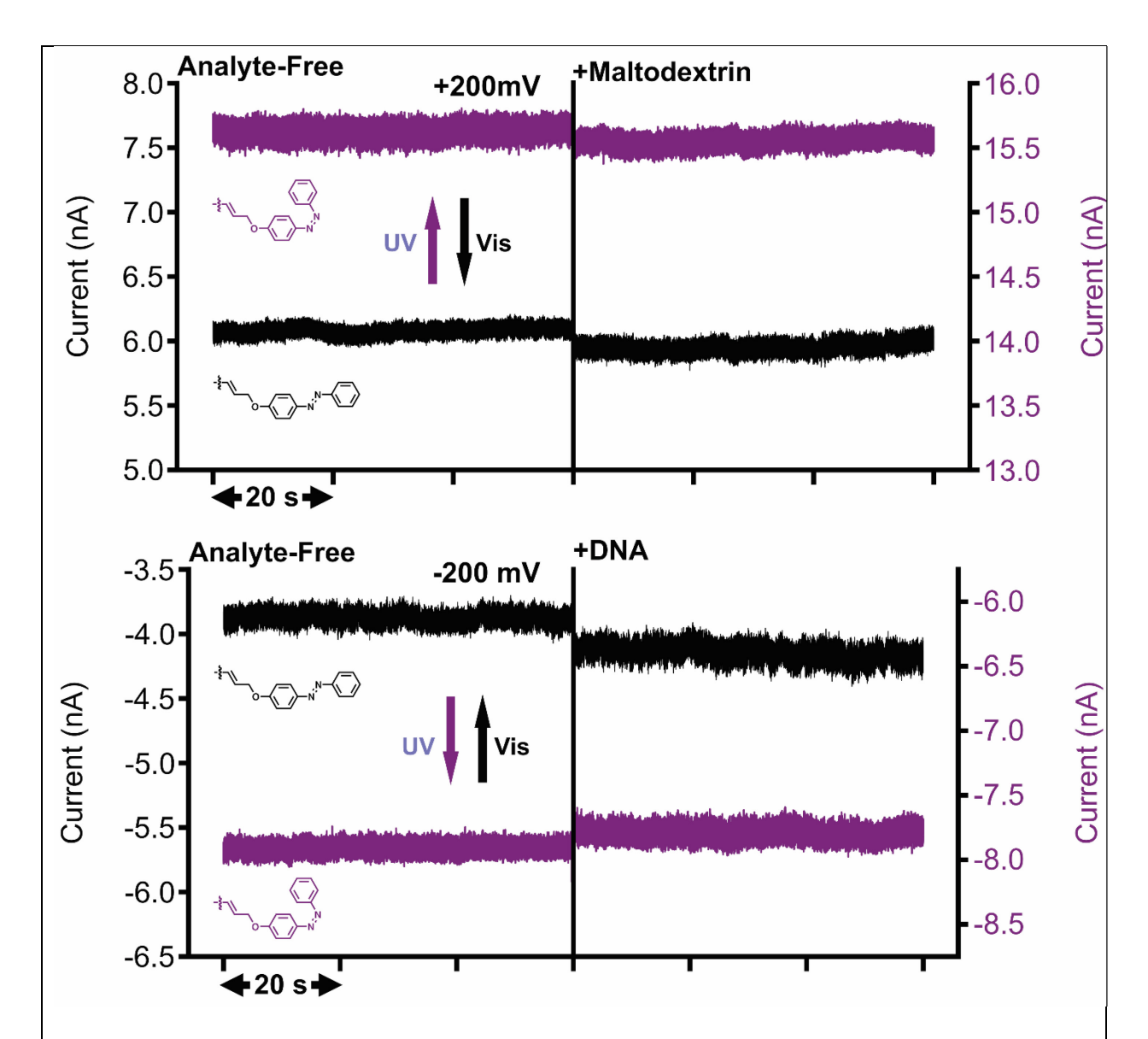


Figure S11. Current traces for the *cis* and *trans* configuration of the nanopore with voltages opposite to those in Figure 2. Current traces were acquired at -200 mV for DNA with a 10.1 nm (7.2 nm) diameter *cis* (*trans*) configuration pore and at +200 mV for maltodextrin with a 14.9 nm (7.6 nm) diameter *cis* (*trans*) configuration pore. The -200 mV voltage polarity would oppose electrophoretic detection of anionic DNA and the +200 mV voltage polarity would oppose electroosmotic detection of neutral maltodextrin. No events were detected at these polarities,

with events being detected at the opposite polarity when the surface coating was in the *cis* configuration.

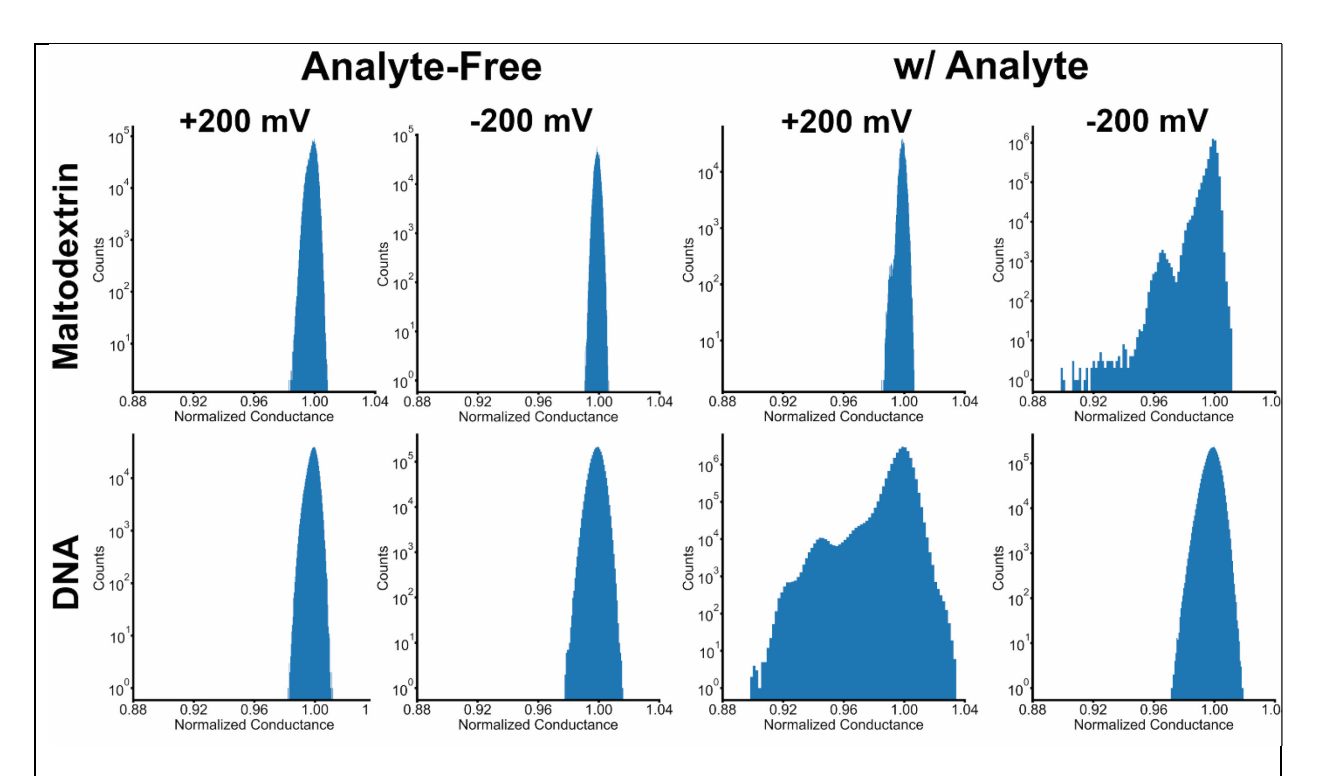


Figure S12. Histograms of the conductance are shown for experiments using a *cis* nanopore with and without analyte and for both voltage polarities. All data shown was collected under a magnitude 200 mV potential in 1 M KCl buffered to pH 7 with 10 mM HEPES. Data was collected using a 14.9 nm diameter *cis* pore (7.6 nm *trans*) for maltodextrin and a ∼10.1 nm diameter *cis* pore (7.2 nm *trans*) for 3 kbp dsDNA. All conductance values recorded in a given run were scaled by the average (by histogram mode) open pore conductance in each analysis window. Measurements in the absence of events were recorded for 5 minutes whereas those where events were detected were recorded for 20 minutes. DNA detection was possible with a +200 mV polarity (the electrophoretic direction) whereas maltodextrin required -200 mV polarity (the electropsomotic direction).

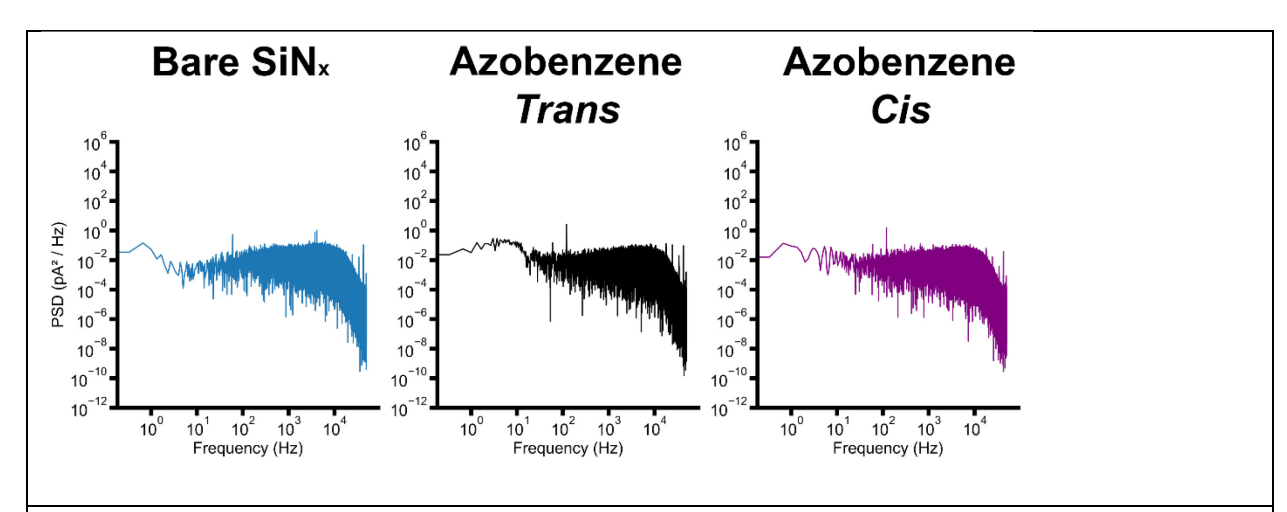


Figure S13. Power spectral density plots for a native SiN_x pore (4.5 nm diameter) and an azobenzene functionalized pore in both *cis* (14 nm diameter) and *trans* (7 nm diameter) configurations. This data represents a 3 s current trace with a 0 V potential collected in 1 M KCl buffered to pH 7 by 10 mM HEPES.

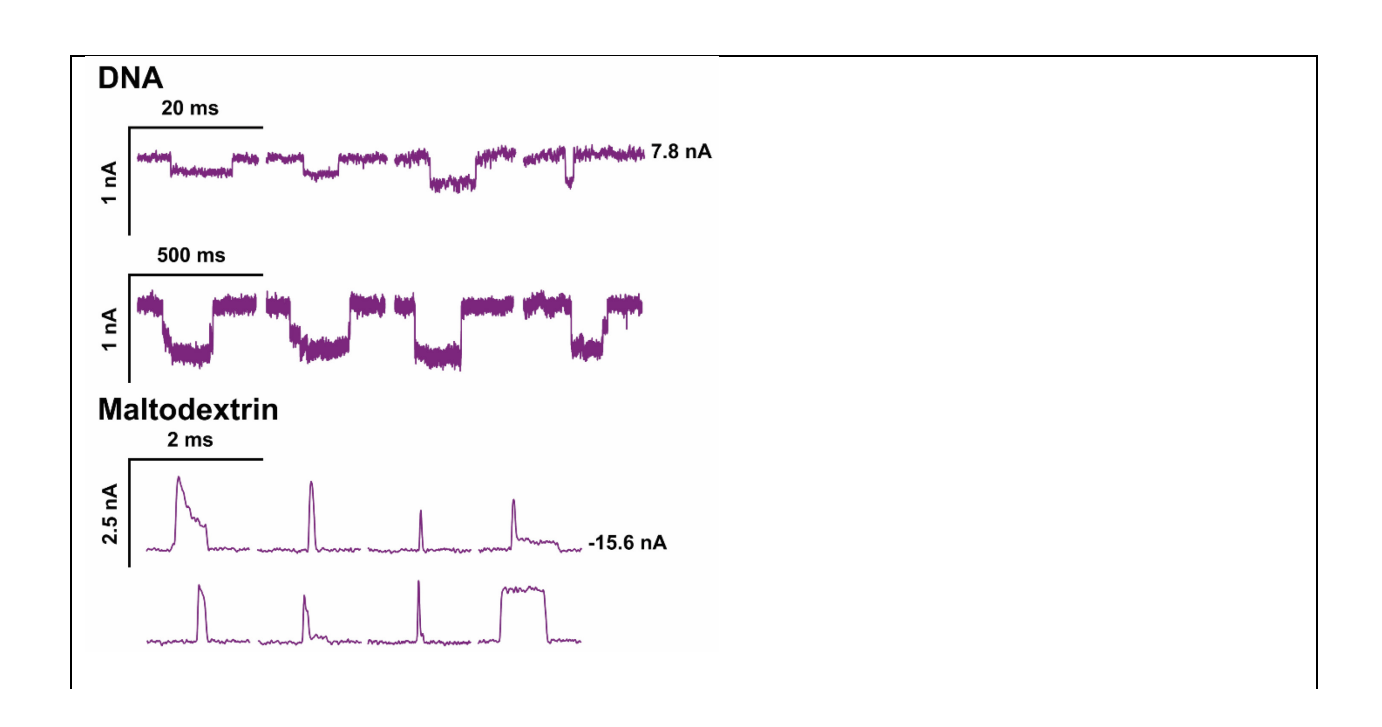


Figure S14. Characteristic events for each analyte in 1 M KCl buffered at pH 7 with 10 mM HEPES (~10.₁ and ~14.₉ nm diameter pores, respectively). Under the experimental conditions the voltage polarity required for electrophoretic detection of the anionic DNA was positive and was negative for electroosmotic detection of the neutral maltodextrin so that the current blockages appear inverted with respect to each other.

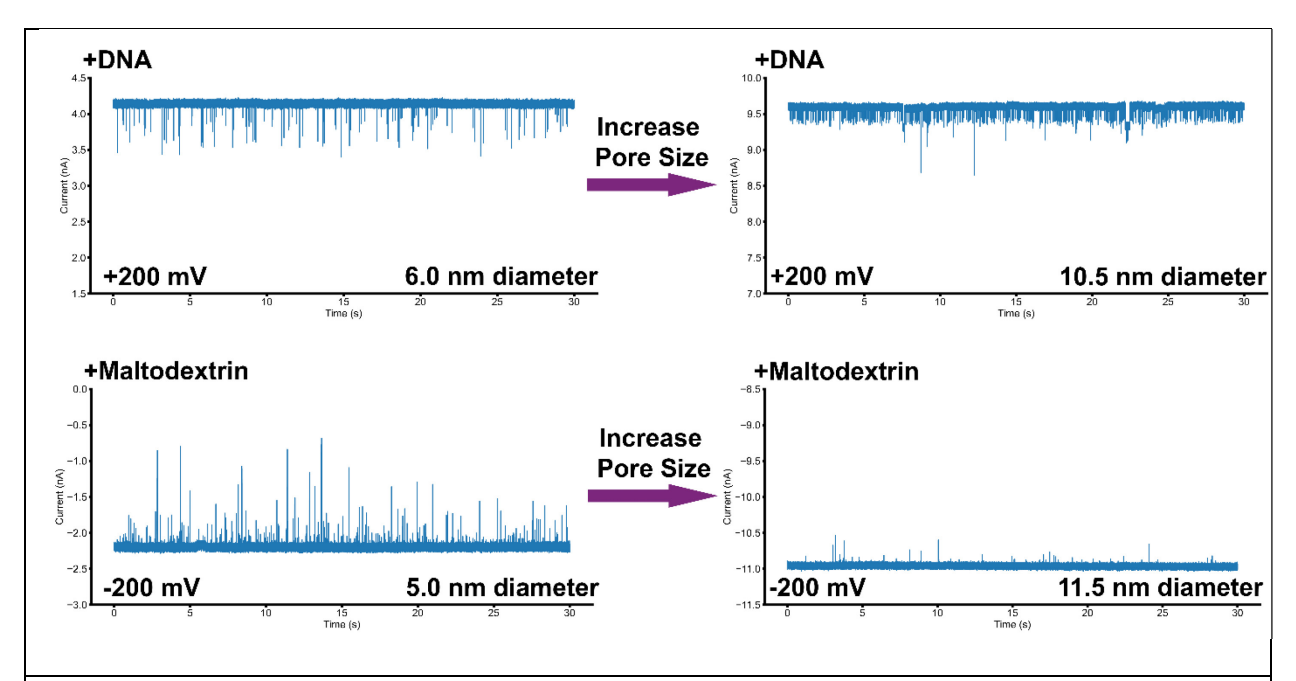


Figure S15. Current traces of 3 kbp dsDNA and maltodextrin analyzed by a native SiN_x pore in 1 M KCl buffered to pH 7 by 10 mM HEPES. Given the good wetting of CBD SiN_x nanopores, the conductance-derived nanopore diameters can be considered an excellent approximation to the physical nanopore diameter. The fractional volume of the nanopore occupied by the analyte dictates the proportion of charge that is physically volume-excluded from the pore.⁶⁴ An increase in nanopore diameter then contributes to a general reduction in the magnitude of the blocked current as a fraction of the open-pore current. Simultaneously, larger pore diameters can allow for sufficiently flexible molecules to adopt conformations that occlude a larger volume of the

nanopore (and thus increase the fractional blockage magnitude) than would a linear conformation.⁶⁴

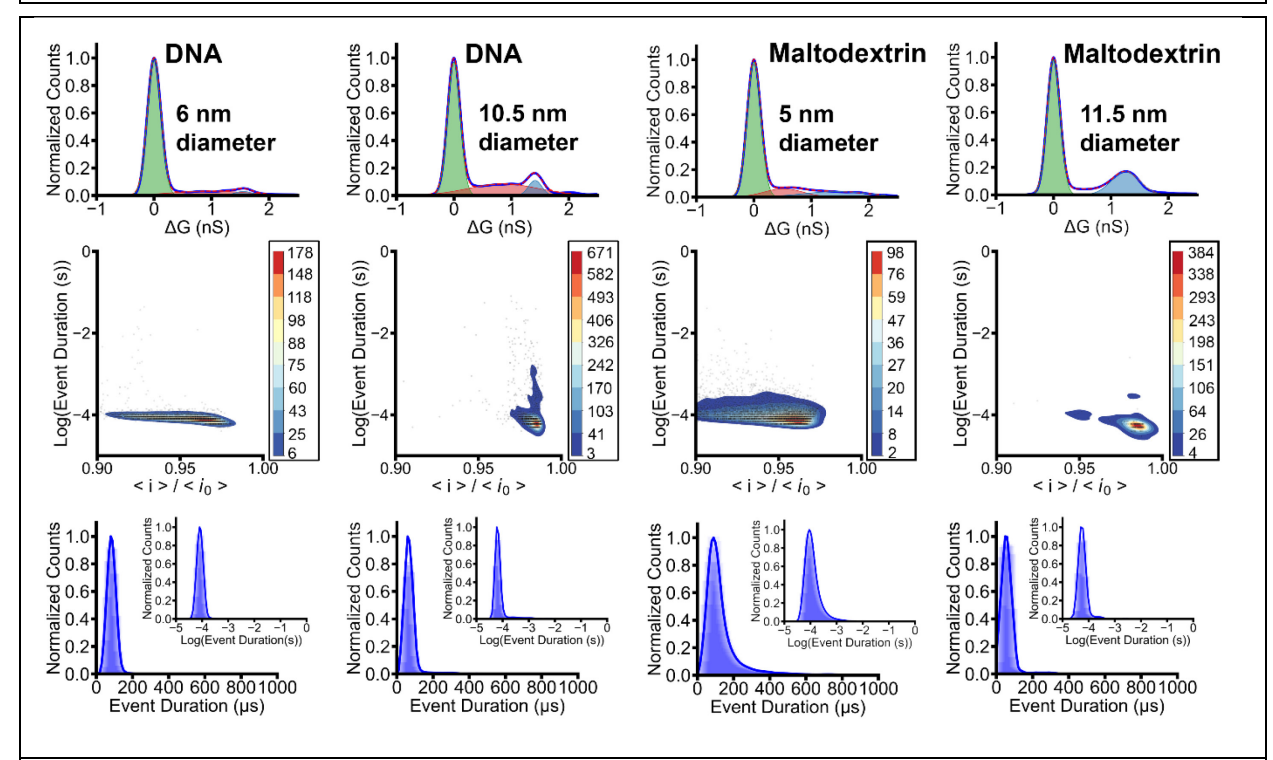


Figure S16. Measurements of 3 kbp dsDNA and maltodextrin were made using two different native (unfunctionalized) SiN_x nanopores with different diameters (*cf.* Figure 3 for measurements using functionalized pores in the *cis* configuration). Individual current blockage events were extracted from current traces as in Figure S15, with DNA sensed at 200 mV using 6.0 and 10.5 nm diameter pores and maltodextrin sensed at -200 mV using 5.0 and 11.5 nm diameter pores. All measurements were in 1 M KCl buffered to pH 7 with 10 mM HEPES. Top row. The average shifted histogram (ASH) of the change in the conductance shows peaks corresponding to the open-pore current at $\Delta G = 0$ nS and analyte-induced blockages (peaked at $\Delta G > 0$). Discrete events were first extracted by thresholding from the baseline and ΔG is measured for each event relative to its local baseline. Middle row. Scatter plots of all isolated events are superimposed with heat maps showing the frequency of events in each analyte. The

abscissa, $\langle i \rangle / \langle i_0 \rangle$, is the mean blockage of each event scaled by the mean open pore current proximal to the event. Bottom row. ASH plots of event duration for all isolated events.

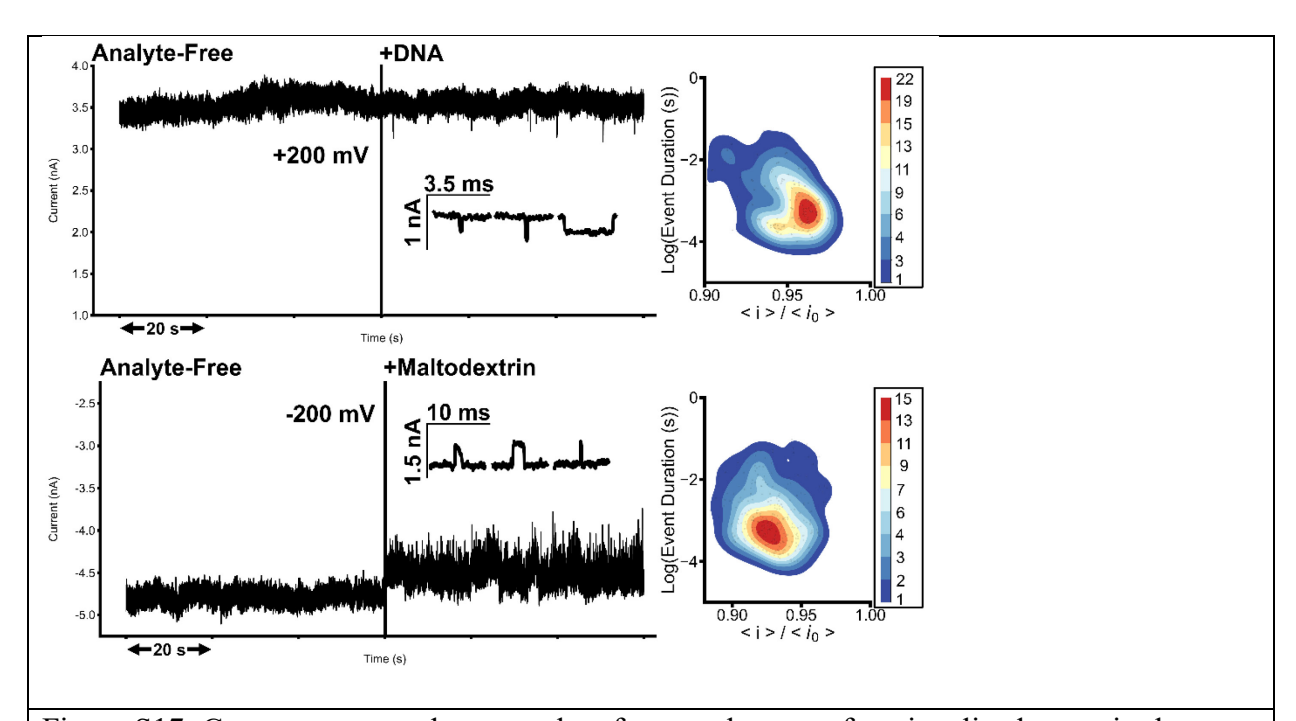


Figure S17. Current traces and scatter plots from azobenzene functionalized pores in the *trans* configuration analyzing 3 kbp dsDNA and maltodextrin in a 1:3 solution of acetonitrile and electrolyte (1 M KCl buffered to pH 7 with 10 mM HEPES). Nanopore sizes were measured in conventional pH 7, 1 M KCl, 10 mM HEPES aqueous solutions before switching to the mixed electrolyte. The effective conductance-derived diameters were 7.0 nm for the DNA measurement (13.5 nm as *cis*), and 7.5 nm for the maltodextrin measurement (10.5 nm as *cis*)—similar to the *trans* pore dimensions in Figure S11.

REFERENCES

- (1) Karawdeniya, B. I.; Bandara, Y. M. N. D. Y.; Nichols, J. W.; Chevalier, R. B.; Dwyer, J. R. Surveying Silicon Nitride Nanopores for Glycomics and Heparin Quality Assurance. *Nat Commun* **2018**, *9*, 3278. DOI: 10.1038/s41467-018-05751-y.
- (2) Waugh, M.; Briggs, K.; Gunn, D.; Gibeault, M.; King, S.; Ingram, Q.; Jimenez, A. M.; Berryman, S.; Lomovtsev, D.; Andrzejewski, L.; Tabard-Cossa, V. Solid-State Nanopore Fabrication by Automated Controlled Breakdown. *Nature Protocols* **2020**, *15*, 122-143. DOI: 10.1038/s41596-019-0255-2.
- (3) Kwok, H.; Briggs, K.; Tabard-Cossa, V. Nanopore Fabrication by Controlled Dielectric Breakdown. *PLoS ONE* **2014**, *9*, e92880. DOI: 10.1371/journal.pone.0092880.
- (4) Bandara, Y. M. N. D. Y.; Karawdeniya, B. I.; Hagan, J. T.; Chevalier, R. B.; Dwyer, J. R. Chemically Functionalizing Controlled Dielectric Breakdown Silicon Nitride Nanopores by Direct Photohydrosilylation. *ACS Appl. Mater. Interfaces* **2019**, *11*, 30411-30420. DOI: 10.1021/acsami.9b08004.
- (5) Xia, K.; Hagan, J. T.; Fu, L.; Sheetz, B. S.; Bhattacharya, S.; Zhang, F.; Dwyer, J. R.; Linhardt, R. J. Synthetic Heparan Sulfate Standards and Machine Learning Facilitate the Development of Solid-State Nanopore Analysis. *P Natl Acad Sci USA* **2021**, *118*, e2022806118. DOI: 10.1073/pnas.2022806118.
- (6) Dassault Systèmes. *Biovia Discovery Studio Visualizer*; Dassault Systèmes: San Diego, 2019. (7) Frisch, M. J.; Truck, G. W.; Schlegel, H. B.; Scuseria, G. E.; Robb, M. A.; Cheeseman, J. R.; Scalmani, G.; Barone, B.; Mennucci, B.; Petersson, G. A.; Nakatsuji, H.; Caricato, M.; Li, X.; Hratchian, H. P.; Izmaylov, A. F.; Bloino, J.; Zheng, G.; Sonnenberg, J. L.; Hada, M.; Ehara, M.; *et al. Gaussian 09*; Gaussian, Inc.: Wallingford CT, 2009.
- (8) Tabard-Cossa, V.; Trivedi, D.; Wiggin, M.; Jetha, N. N.; Marziali, A. Noise Analysis and Reduction in Solid-State Nanopores. *Nanotechnology* **2007**, *18*. DOI: http://dx.doi.org/10.1088/0957-4484/18/30/305505.